

Joint analysis of functional genomic data and genome-wide
association studies of 18 human traits

Joseph K. Pickrell^{1,2}

¹ New York Genome Center, New York, NY

² Department of Biological Sciences, Columbia University, New York, NY

Correspondence to: jkpickrell@nygenome.org

June 16, 2022

Abstract

Annotations of gene structures and regulatory elements can inform genome-wide association studies (GWAS). However, choosing the relevant annotations for interpreting an association study of a given trait remains challenging. We describe a statistical model that uses association statistics computed across the genome to identify classes of genomic element that are enriched or depleted for loci that influence a trait. The model naturally incorporates multiple types of annotations. We applied the model to GWAS of 18 human traits, including red blood cell traits, platelet traits, glucose levels, lipid levels, height, BMI, and Crohn's disease. For each trait, we evaluated the relevance of 450 different genomic annotations, including protein-coding genes, enhancers, and DNase-I hypersensitive sites in over a hundred tissues and cell lines. We show that the fraction of phenotype-associated SNPs that influence protein sequence ranges from around 2% (for platelet volume) up to around 20% (for LDL cholesterol); that repressed chromatin is significantly depleted for SNPs associated with several traits; and that cell type-specific DNase-I hypersensitive sites are enriched for SNPs associated with several traits (for example, the spleen in platelet volume). Finally, by re-weighting each GWAS using information from functional genomics, we increase the number of loci with high-confidence associations by around 5%.

1 Introduction

A fundamental goal of human genetics is to create a catalogue of the genetic polymorphisms that cause phenotypic variation in our species and to characterize the precise molecular mechanisms by which these polymorphisms exert their effects. An important tool in the modern human genetics toolkit is the genome-wide association study, in which hundreds of thousands or millions of single nucleotide polymorphisms (SNPs) are genotyped in large cohorts of individuals and each polymorphism tested for a statistical association with some trait of interest. In recent years, GWAS have identified thousands of genomic regions that show reproducible statistical associations with a wide array of phenotypes and diseases¹.

In general, the loci identified in GWAS of multifactorial traits have small effect sizes and are located outside of protein-coding exons². This latter fact has generated considerable interest in annotating other types of genomic elements apart from exons. For example, the ENCODE project has generated detailed maps of histone modifications and transcription factor binding in six human cell lines, partially motivated by the goal of interpreting GWAS signals that may act via a mechanism of gene regulation³. Methods for combining potentially rich sources of functional genomic data with GWAS could in principle lead to important biological insights. The development of such a method is the aim of this paper.

There are two lines of research that motivate our work on this problem. The first is what are often called “enrichment” analyses. In this type of analysis, the most strongly associated SNPs in a GWAS are examined to see if they fall disproportionately in specific types of genomic region. These studies have found, for example, that SNPs identified in GWAS are enriched in protein-coding exons, promoters, and untranslated regions (UTRs)^{2;4} and among those that influence gene expression^{5;6}. Further, in some cases, SNPs associated with a trait are enriched in gene regulatory regions in specific cell types⁷⁻¹⁸ or near genes expressed in specific cell types^{19;20}. However, the methods in these studies are generally not able to consider more than a single annotation at a time (with a few exceptions^{21;22}). Further, they are not set up to answer a question that we find important: consider two independent SNPs with equivalent P-values of 1×10^{-7} in a GWAS for some trait (note that this P-value does not reach the standard threshold of 5×10^{-8} for “significance”), the first of which is a nonsynonymous SNP and the second of which falls far from any known gene. What is the probability that the first SNP is truly associated with the trait, and how does this compare to the probability for the second?

A potential answer to this question comes from the second line of research that motivates this work. In association studies where the phenotype being studied is gene expression (“eQTL” studies, for “expression quantitative trait locus”), statistical models have been developed to identify shared characteristics of SNPs that influence gene expression²³⁻²⁵. In a hierarchical modeling framework, the probability that a given SNP influences gene expression can then depend on these characteristics. The key fact that makes these models useful in the context of eQTL mapping is that there is a large number of unambiguous eQTLs in the genome on which a model can be trained. In the GWAS context, the number of loci unambiguously associated with a given trait

has historically been very small; learning the shared properties of two or three loci is not a job well-suited to statistical modeling. However, large meta-analyses of GWAS now regularly identify tens to hundreds of independent loci that influence a trait (e.g. ^{26;27}). The merits of hierarchical modeling in this context²⁸⁻³⁰ are thus worth revisiting. Indeed, Carbonetto and Stephens³¹ have reported success in identifying loci involved in autoimmune diseases using a hierarchical model that incorporates information about groups of genes known to interact in a pathway.

In this paper we present a hierarchical model for jointly analyzing GWAS and genomic annotations. We applied this model to GWAS of 18 diseases and traits; for each trait, we learned the relevant types of genomic information from a set of 450 genome annotations.

2 Results

We assembled a set of 18 GWAS with publicly available summary statistics and a large number (at least around 20) of loci associated with the trait of interest. These included studies of red blood cell traits¹⁵, platelet traits³², Crohn’s disease³³, BMI³⁴, lipid levels²⁷, height²⁶, bone mineral density³⁵ and fasting glucose levels³⁶. We used ImpG³⁷ to impute the summary statistics from each study for all common SNPs identified in European populations by the 1000 Genomes Project³⁸. Overall we successfully imputed association statistics for around 80% of common SNPs (Supplementary Figure 1). We then assembled a set of genome annotations, paying specific attention to annotations available for many cell types since important regulatory elements may be active only in specific cell types. The main sources of genome annotations were 402 maps of DNase-I hypersensitivity in a wide range of primary cell types and cell lines^{11;39}. We also included as annotations the output from “genome segmentation” of the six main ENCODE cell lines⁴⁰; for each section of the genome in each cell line, Hoffman et al.⁴⁰ report whether the histone modifications in the region are consistent with enhancer activity, transcription start sites, promoter-flanking regions, CTCF binding sites, or repressed chromatin. Finally, we included elements of gene structures (protein-coding exons and 3’ and 5’ UTRs). In total, we used data from 18 traits and 450 genomic annotations.

For each trait, we set out to identify which of the 450 annotations (if any) were enriched in genetic variants influencing the trait. To do this, we developed a hierarchical model that learns the shared properties of loci influencing a trait. The full details of the model are presented in the Methods, but can be summarized briefly. Conceptually, we break the genome into large, non-overlapping blocks (with an average size of 2.5 Mb). Let the prior probability that any block k contains an association be Π_k . If there is an association in block k , then let the prior probability that any SNP i is the causal SNP be π_{ik} . We allow both Π_k and π_{ik} to depend on annotations of the region and SNP, respectively, and estimate these quantities based on the patterns of enrichment across the whole genome. We tested this approach using simulations based on real data from a GWAS of height (Supplementary Material).

The methodology is best illustrated with an example. We started with an analysis of a GWAS of high-density lipoprotein (HDL) levels²⁷. We first took each genomic annotation individually, and estimated its level of enrichment (or depletion) for loci that influence HDL (in the model, we

additionally included a regional effect of gene density and a SNP-level effect of distance to the nearest transcription start site, see the Methods for details). In Figure 1A, we show the top 40 annotations, ordered by how well each improves the fit of the model. Loci that influence HDL are most strongly enriched in enhancers identified in the HepG2 cell line, and most strongly depleted from genomic regions repressed in that same cell line. HepG2 cells are derived from a liver cancer; the relevance of this cell line to a lipid phenotype makes intuitive sense. However, there are many other additional (correlated) genome annotations that are enriched for loci that influence HDL (Figure 1A). We thus built a model including multiple annotations; to mitigate over-fitting in this situation we used a cross-validation approach (Methods). The best-fitting model is shown in Figure 1B. It includes both enhancers and repressed chromatin identified in HepG2 cells, as well as coding exons and chromatin repressed in K562 cells. Since many of the annotations are correlated, those included in the combined model are the “best” representatives of sets of related annotations. We thus used conditional analysis to define the set of annotations represented by each member of the combined model (Methods; Figure 1A).

A convenient side effect of fitting an explicit statistical model relating properties of SNPs to the probability of association is that we can use the functional information to re-weight the GWAS (Methods). We used the combined model for HDL to re-weight the association statistics across the genome (Figure 1C). There are several regions of the genome with strong evidence for association with HDL (posterior probability of association [PPA] over 0.9) only when using the model incorporating functional information. In Figure 2, we show one such region, near the gene NR0B2. The model identifies the SNP rs6659176 as the most likely candidate to be the causal polymorphism in this region. This SNP has a P-value of 1.5×10^{-6} . However, this SNP falls in a coding exon (in fact it is nonsynonymous), leading the model to conclude that this P-value is in fact strong evidence for association. Indeed, larger studies of HDL have confirmed the evidence for association in this region (P-value of 9.7×10^{-16} at rs12748152, which has $r^2 = 0.85$ with rs6659176¹⁷). This region, though not this particular SNP, was also identified in a scan for SNPs influencing multiple lipid phenotypes⁴¹.

We applied this method to all 18 traits. We were first interested in estimating the fraction of associations for each trait that can be explained by nonsynonymous polymorphisms versus polymorphisms that do not influence protein sequences. For each trait, we fit a model including promoters (SNPs within 5kb of a transcription start site) as well as nonsynonymous polymorphisms. For all traits, nonsynonymous polymorphisms are enriched among those that influence the trait, though this enrichment is not statistically significant for all traits (Figure 3A). This contrasts with synonymous polymorphisms, which are generally not enriched for polymorphisms that influence traits, with a few notable exceptions (like height and Crohn’s disease, see Supplementary Figure 3). We then used these enrichments to estimate the fraction of associations for each trait that are driven by nonsynonymous polymorphisms (Supplementary Material). This fraction varies from around 2% to around 20%, with an average of 10% (Figure 3B). We conclude that the relative importance of changes in protein sequence versus gene expression likely varies across traits.

We then used all 450 genome annotations to build models of enrichment for each trait. As for

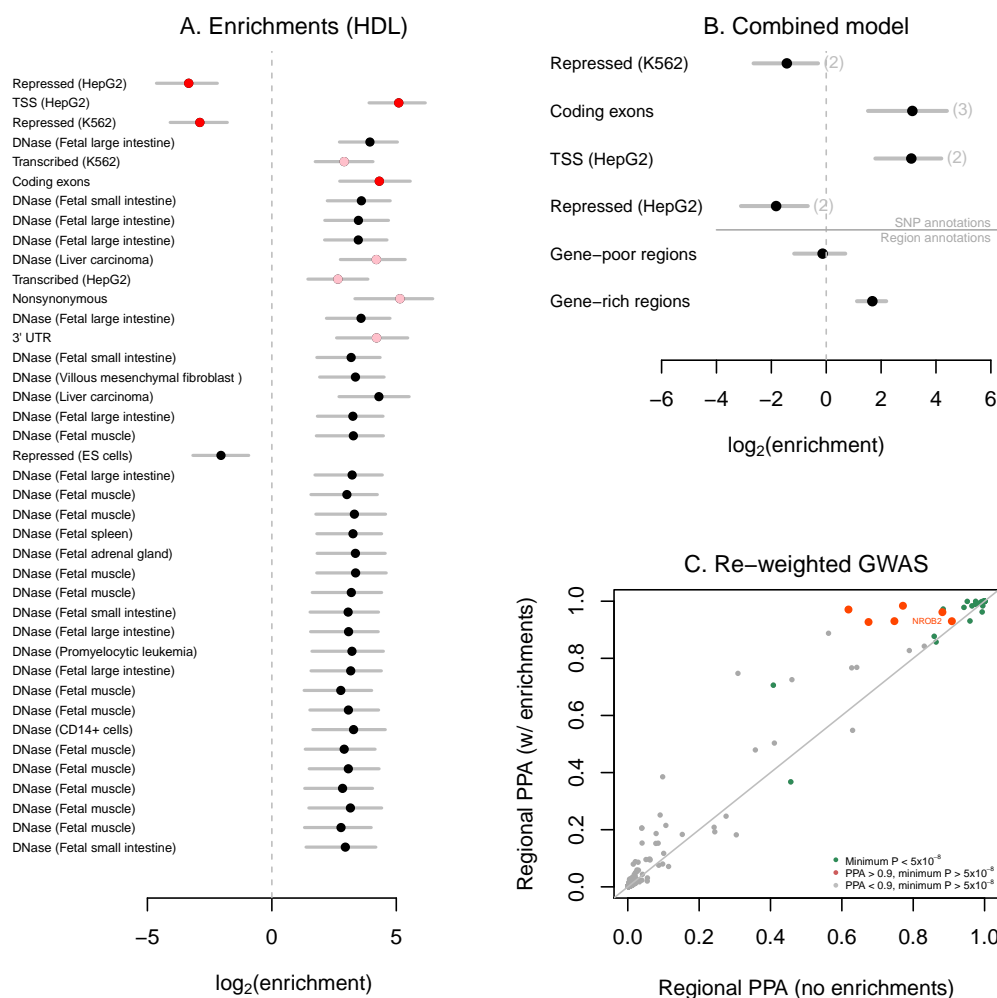


Figure 1. **Application of the model to HDL cholesterol.** **A. Single-annotation models.** We fit the model to each annotation individually, including a SNP-level effect for SNPs 0-5kb from a TSS, a SNP-level effect for SNPs 5-10kb from a TSS, a region-level effect for regions in the top third of gene density, and a region-level effect for regions in the bottom third of gene density. Plotted are the maximum likelihood estimates and 95% confidence intervals of the enrichment parameter for each annotation. Annotations are ordered according to how much they improve the likelihood of the model (at the top are those that improve the likelihood the most). In red are the annotations included in the joint model, and in pink are the annotations that are statistically equivalent to those included in the combined model. **B. Joint model.** Using the algorithm described in the Methods we built a model combining multiple annotations. Shown are the maximum likelihood estimates and 95% confidence intervals of the enrichment effects of each annotation. Note that though these are the maximum likelihood estimates, model choice was performed using a penalized likelihood. In parentheses next to each annotation (except for those relating to distance to transcription start sites), we show the total number of annotations that are statistically equivalent to the included annotation in a conditional analysis. **C. Re-weighted GWAS.** We re-weighted the GWAS using the model with all the annotations in **B** (under the penalized enrichment parameters from Supplementary Table 9). Each point represents a region of the genome, and shown are the posterior probabilities of association (PPA) of the region in the models with and without the annotations.

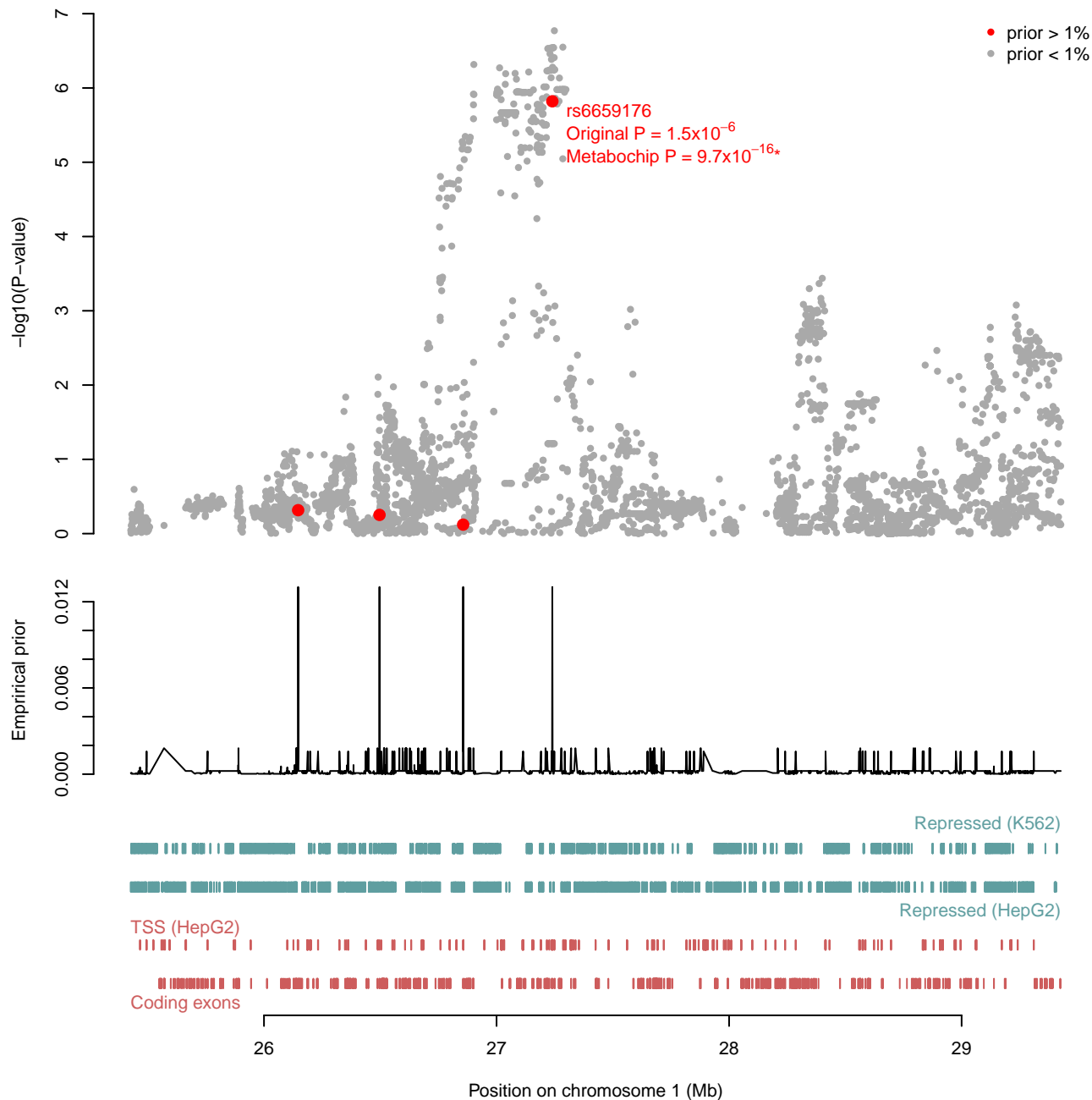
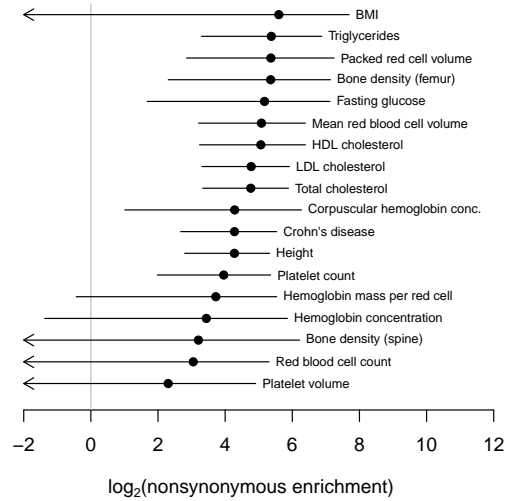


Figure 2. **Regional plot surrounding NR0B2.** In the top panel we plot the P-values for association with HDL levels at each SNP in this region. In the middle panel is the fitted empirical prior probability that each SNP is the causal one in the region, conditional on there being a single causal SNP in the region. This prior was estimated using the combined model with the annotations in Figure 1B. In the lower panel are the positions of the annotations included in the model.* The reported P-value is for rs12748152, which has $r^2 = 0.85$ with rs6659176.

A. Enrichment of nonsynonymous SNPs among GWAS hits



B. Proportion of associated SNPs that are nonsynonymous

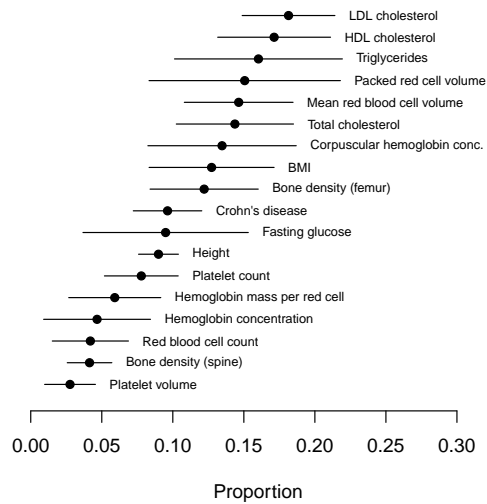


Figure 3. **Estimated role of protein-coding changes in each trait.** **A. Estimated enrichment of non-synonymous SNPs.** For each trait, we fit a model including an effect of non-synonymous SNPs and an effect of SNPs within 5kb of a TSS. Shown are the estimated enrichment parameters and 95% confidence intervals for the non-synonymous SNPs. **B. Estimated proportion of GWAS hits driven by non-synonymous SNPs.** For each trait, using the model fit in **A.**, we estimated the proportion of GWAS signals driven by non-synonymous SNPs. Shown is this estimate and its standard error (Supplementary Material).

HDL, we first estimated enrichment levels individually for each annotation (Supplementary Figures 4-12). Clustering of phenotypes according to these enrichment levels recapitulated many known relationships between traits (Supplementary Figure 13). We then generated a combined model for each trait. The parameters of the combined models are shown in Figure 4 and Supplementary Figure 14, and details of the exact annotations are in Supplementary Tables 2-20. In general, the models generated with this method are sparse and biologically interpretable. A few general patterns emerge from this analysis. Apart from the repeated occurrence of annotations related to protein-coding genes, marks of repressed chromatin are often significantly depleted for SNPs influencing traits. For example, SNPs influencing Crohn’s disease are depleted from repressed chromatin identified in a lymphoblastoid cell line (Figure 4D; \log_2 enrichment of -1.83, 95% CI [-3.06, -0.78]), SNPs influencing height are significantly depleted from repressed chromatin in HeLa cells (Figure 4I; \log_2 enrichment of -1.5, 95% CI [-2.39, -0.71]), and SNPs influencing red blood cell volume are significantly depleted from repressed chromatin in an erythroblast-derived cell line (Figure 4F; \log_2 enrichment of -3.91, 95% CI [-6.25, -2.38]).

We additionally observed cell type-specific enrichments in enhancer elements and DNase hypersensitive sites for SNPs that influence traits. Most of the observed enrichments are readily interpreted in light of the known biology of the trait. For example, SNPs that influence platelet volume and platelet count are enriched in open chromatin identified in CD34⁺ cells, known to be on the cell lineage that leads to platelets⁴² (Figure 4A,B; \log_2 enrichment of 1.81, 95% CI [0.59, 2.86] for platelet count; \log_2 enrichment of 3.02, 95% CI [1.69, 4.26] for platelet volume); and SNPs that influence corpuscular hemoglobin concentration are enriched in open chromatin identified in K562 cells, a cell line derived from a cancer of erythroblasts (Supplementary Figure 14E; \log_2 enrichment of 2.67, 95% CI [0.61, 4.44]). For some traits, however, the connection between the trait and the tissues identified is not immediately obvious. For example, SNPs associated with platelet density are enriched in open chromatin in the spleen (Figure 4A; \log_2 enrichment of 1.93, 95% CI [0.59, 3.14]), and SNPs associated with height are enrichment in open chromatin in muscle (Figure 4I; \log_2 enrichment of 2.27, 95% CI [1.51, 3.02]); note that though there are all a large number of annotations equivalent to this annotation of open chromatin in fetal muscle, all of them are muscle-related; see Supplementary Figure 5B).

For two traits—Crohn’s disease (Figure 4D) and red blood cell count (Supplementary Figure 14G)—we noticed that annotations initially identified as enriched for SNPs influencing the trait ended up in the combined model as being depleted for SNPs influencing the trait. On further examination (Supplementary Material), we found that these effects are due to statistical interactions. For example, when treated alone, SNPs that influence Crohn’s disease are enriched in DNase-I hypersensitive sites identified in fetal fibroblasts from the abdomen (\log_2 enrichment of 3.17, 95% CI [1.66, 4.36]). However, DNase-I hypersensitive sites identified in fetal fibroblasts from the back show an even stronger enrichment (\log_2 enrichment of 4.21, 95% CI [2.99, 5.29]), and sites in common between the two annotation are intermediate (\log_2 enrichment of 3.74, 95% CI [2.29, 4.89]). This leads to an interaction where in the joint model the contribution of the DNase-I hypersensitive sites identified in fetal abdominal fibroblasts is negative. Though this is a statistical

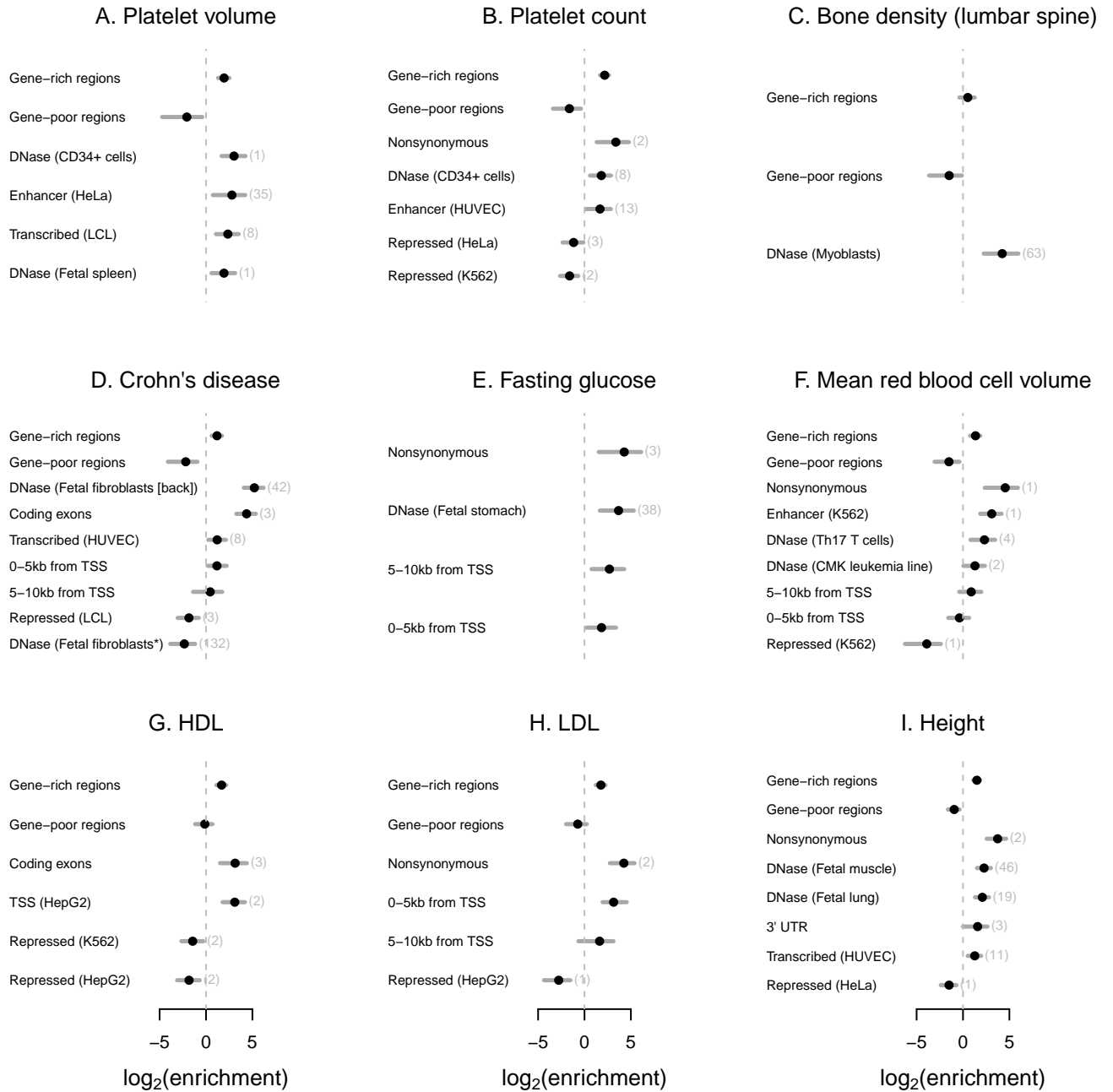


Figure 4. **Combined models for nine traits.** For each trait, we built a combined model of annotations using the algorithm presented in the Methods. Shown are the maximum likelihood estimates and 95% confidence intervals for all annotations included in each model. Note that though these are the maximum likelihood estimates, model choice was done using a penalized likelihood (Methods). For the other nine traits, see Supplementary Figure 14. In parentheses next to each annotation (except for those relating to distance to transcription start sites), we show the total number of annotations that are statistically equivalent to the included annotation in a conditional analysis (Methods). *This annotation of DNase-I hypersensitive sites in fetal fibroblasts from the abdomen has a positive effect when treated alone; see the text for discussion.

explanation for this observation, the biological explanation is not immediately clear. It seems likely that DNase-I hypersensitive sites are a heterogeneous set of different classes of elements, and that different experiments are more sensitive, for either technical or biological reasons, to subsets of these elements.

Finally, we explored the potential of this model to identify new loci (as in Figure 2). In order to do this, one needs a threshold for “significance” in this model, ideally with similar properties as the standard P-value threshold of 5×10^{-8} . To calibrate the method, we used the fact that we initially applied our method to a study of four lipid traits that identified about 100 loci in a sample size of around 90,000 individuals²⁷. Since then, larger studies have raised the number of loci associated with lipid traits to 157¹⁷. If we treat a locus with a P-value of 5×10^{-8} in the larger study as a “true positive” and a locus that does not reach this threshold in the larger study as a “true negative”, we can calibrate a threshold for posterior probability of association using the replication data (Supplementary Material). We found that a threshold of a regional PPA of 0.9 performed similarly to a stringent P-value threshold (Supplementary Figure 15). Combining the loci from both the standard P-value approach and our approach resulted in an approximately 5% increase in the number of identified loci while still maintaining a false positive rate close to zero (Supplementary Figure 15, Supplementary Table 21). This is only a modest gain in power; that said, by applying this method to all 18 traits we identified 49 loci that did not reach a standard statistical significance threshold of 5×10^{-8} but have a PPA over 0.9 (Supplementary Table 22). Based on the above results for lipids, the level of evidence that these loci are true positives is approximately the same as those that have $P = 5 \times 10^{-8}$ in a standard GWAS. Indeed, the majority of these loci have since been identified in larger cohorts than those used in this paper (Supplementary Table 22).

3 Discussion

In this paper, we have developed a statistical model for identifying genomic annotations that are most relevant to the biology of a given phenotype. We have shown that this model is able to scan through hundreds of genomic annotations to identify a sparse set of biologically-interpretable annotations without prior knowledge of the biology of the phenotype.

Linking GWAS to biology

Perhaps the most striking observation is that chromatin annotated as repressed in a given cell type is often depleted for SNPs that influence traits. Since approximately 60-70% of the genome falls in this annotation in any given cell type (Supplementary Material), this information could dramatically limit the number of SNPs considered when fine-mapping loci identified in GWAS. Additionally, we identified several non-obvious connections between tissue and phenotypes. For example, SNPs that influence platelet volume are enriched in DNase-I hypersensitive sites in the spleen (Figure 4A). Though the spleen functions in the removal of platelets from the bloodstream, the connection between its function and platelet volume is unclear. An important next step will be

to connect the identified non-coding variants in regulatory regions to changes in gene expression, which is presumably the mechanism by which they exert an effect on phenotypes. Methods for inferring the casual chain between variation in DNase-I sensitivity, variation in gene expression, and variation in phenotypes (e.g.^{41;43–46}) will be essential.

Modeling assumptions

We have made several modeling assumptions that merit discussion. First, by splitting the genome into blocks based on numbers of SNPs, we are making the implicit assumption that the probability that a genomic region contains a SNP associated with a given phenotype depends on the SNP density rather than the physical size—that is, a short genomic region with a large number of SNPs is *a priori* as likely to have an association as a long genomic region with few SNPs. We have also made a more restrictive assumption that there can be only a single causal SNP in a given genomic region. This assumption is a natural starting point, but as GWAS sample sizes increase even more it will begin to be untenable. Advances in methods for joint analysis of multiple SNPs (e.g. Yang et al.⁴⁷) may provide a way forward in this situation. Finally, we note that the model is limited by the types of genomic annotations that are available, and the best annotations identified in the model may be “proxies” for the truly-relevant annotations. For example, SNPs associated with height are enriched in DNase-I hypersensitive sites identified in the fetal lung (Figure 4I); taken literally, this would suggest that some SNPs influence height through lung development. An alternative possibility, however, is that patterns of open chromatin in the lung (which is of course a heterogeneous tissue) are useful proxies for patterns of open chromatin in a cell type that has not been profiled; this hypothetical cell type could in principle be present in any tissue.

Prospects for fine-mapping GWAS loci using functional genomic data

We have primarily focused on using our model to identify annotations relevant to a trait of interest, though we have also explored using this information to identify novel loci. A third natural application, which we have not explored, is the possibility for fine-mapping GWAS loci using functional genomic information⁴⁸. Indeed, the posterior probability that each SNP in a given genomic region is the causal one is explicitly included in our model. However, in current applications around 20% of common SNPs are neither genotyped nor successfully imputed; this is a major limitation to fine-mapping that cannot be overcome with statistical means. As GWAS move to even denser genotyping or sequencing, we expect that re-visiting this issue will be fruitful.

Methods

In this section we detail the specifics of the hierarchical model; a description of the data used is in the Supplementary Material. The model we propose is most closely related to that developed by Veyrieras et al.²³ in the context of eQTL mapping. Conceptually, we split the genome into independent blocks, such that the blocks are larger than the extent of LD in the population. We

then allow each block to contain either a single polymorphism that causally influences the trait or none. We model the prior probability that any given block contains an association and the conditional prior probability that any given SNP in the block is the causal one. The key is that we allow these probabilities to vary according to functional annotations—for example, gene-rich regions might be more likely to contain associations, and if there is an association, the causal polymorphism may be more likely to fall in a transcription factor binding site. We then estimate these priors using an empirical Bayes approach. Software implementing this model is available at <https://github.com/joepickrell/fgwas>.

Computing the Bayes factor

The basic building block of the model is a linear regression model. Consider a single SNP genotyped in N phenotyped individuals. Assume each individual has an associated measurement of a quantitative trait (we describe a slight modification for case-control studies later), and let \vec{y} be the vector of phenotypes. Let \vec{g} be the vector of genotypes (coded 0, 1, or 2 according to counts of an arbitrarily-defined allele). We use a standard additive linear model:

$$E[y_i] = \alpha + \beta g_i. \quad (1)$$

We would like to compare two models: one where $\beta = 0$ and one where $\beta \neq 0$. A natural way to compare these two models is the Bayes factor:

$$BF = \frac{\int P(\vec{y}|\vec{g}, H_1)}{\int P(\vec{y}|\vec{g}, H_0)}, \quad (2)$$

where H_1 and H_0 represent the parameters of the the alternative and null models, respectively, and which are integrated out.

To compute Equation 2, we use the approximate Bayes factor from Wakefield⁴⁹. This Bayes factor has the practically important property that it can be calculated from a summary of the linear regression, without access to the underlying genotype vector \vec{g} . For completeness, we re-iterate here the underlying model. If $\hat{\beta}$ is the maximum likelihood estimator of β and \sqrt{V} is the standard error of $\hat{\beta}$, Wakefield⁴⁹ suggests a model in which:

$$\hat{\beta} \sim N(\beta, V). \quad (3)$$

Wakefield⁴⁹ places a normal prior on β , such that $\beta \sim N(0, W)$. Under this model Equation 2 becomes:

$$BF = \frac{\sqrt{1-r}}{\exp[-\frac{Z^2}{2}r]}, \quad (4)$$

where $r = \frac{W}{V+W}$ and $Z = \frac{\hat{\beta}}{\sqrt{V}}$ (a standard Z-score). Thus, from a Z-score, an estimate of V , and the prior variance W , we can obtain a Bayes factor measuring the statistical support for a model

in which a SNP is associated with a trait as compared to a model in which a SNP is not associated with a trait. Note, however, that because of linkage disequilibrium in the genome, any true causal association will lead to multiple true statistical associations. In all applications, we set $W = 0.1$ as the prior, such that the majority of the weight of the prior is on small effect sizes (results are robust to some variation in this prior; see Supplementary Material and Supplementary Figure 16).

Hierarchical model

Now consider a set of M SNPs, each of which has been genotyped in N individuals in a GWAS. Our goal is to build a model to identify the shared characteristics of SNPs that causally influence a trait. Because of LD, there will be many associations in the genome that are not causal; however, these will all be restricted to a block around the truly causal site. We thus split the genome into contiguous blocks of size K SNPs (in all of our applications, we set $K = 5,000$, though doubling this block size had little effect on the results; see Supplementary Material and Supplementary Figure 16), such that there are M/K blocks. We choose the block size to be much larger than the extent of linkage disequilibrium in the population. Let Π_k be the prior probability that block k contains a causal SNP associated with the trait. The probability of the data (the set of observed phenotypes) is then:

$$P(\vec{y}) = \prod_{k=1}^{M/K} (1 - \Pi_k)P_k^0 + \Pi_k P_k^1, \quad (5)$$

where P_k^0 is the probability of the data in block k under the model where there are no SNPs associated with the trait in the block, and P_k^1 is the probability of the data in block k under the model where there is one SNP associated with the trait in the block. Further,

$$P_k^1 = \sum_{i \in S_k} \pi_{ik} P_{ik}^1, \quad (6)$$

where S_k is the set of SNPs in block k , π_{ik} is the prior probability that SNP i is the causal SNP in the region conditional on there being an association in block k , and P_{ik}^1 is the probability of the data under the model where this SNP is associated with the trait. Note that this is not a multiple regression model where we jointly model the effects of multiple SNPs on a trait (as in, for example, Carbonetto and Stephens³¹).

We can now allow the prior probabilities—both Π_k (the prior on the block of SNPs containing an association) and π_{ik} (the prior probability that SNP i is the causal SNP assuming there is a single association in block k)—to depend on external information. We would also like to avoid subjective variation in Π_k and π_i , but instead learn from the data itself which genomic annotations are most important. Specifically, we model the regional prior probability as:

$$\ln \left(\frac{\Pi_k}{1 - \Pi_k} \right) = \kappa + \sum_{l=1}^{L_1} \gamma_l I_{kl}, \quad (7)$$

where L_1 is the number of region-level annotations in the model, γ_l is the effect associated with annotation l and I_{kl} takes the value 1 if region k is annotated with annotation l and 0 otherwise. For example, in practice we will estimate a γ parameter for regions of high or low gene density. We then model the SNP prior probability as:

$$\pi_{ik} = \frac{e^{x_i}}{\sum_{j \in S_k} e^{x_j}}, \quad (8)$$

where

$$x_i = \sum_{l=1}^{L_2} \lambda_l I_{il}, \quad (9)$$

where L_2 is the number of SNP-level annotations in the model, λ_l is the effect of SNP annotation l and I_{il} takes the value 1 if SNP i falls in annotation l and 0 otherwise. For example, in practice we will estimate a λ parameter for nonsynonymous SNPs.

Fitting the model

Combining terms above, we see that the likelihood of the data can be written down as:

$$L(\vec{y}|\theta) = \prod_{k=0}^{M/K} (1 - \Pi_k) P_k^0 + \Pi_k \sum_{i=0}^K \pi_{ij} P_{ik}^1 \quad (10)$$

$$= \prod_{k=0}^{M/K} P_k^0 [(1 - \Pi_k) + \Pi_k \sum_{i=0}^K \pi_{ik} B F_i], \quad (11)$$

where θ contains all the parameters of the model, most notably the set of annotation parameters. We maximize this function using the Nelder-Mead algorithm implemented in the GNU Scientific Library.

Shrinkage estimators of the annotation parameters

While maximizing Equation 10 gives the maximum likelihood estimates of all parameters, one concern is that there may be some level of overfitting. When comparing models, we instead shrink these parameters towards zero. Specifically, we define a penalized log-likelihood function:

$$l^*(\vec{y}|\theta) = \ln\left(L(\vec{y}|\theta)\right) - p\left(\sum_{l=1}^{L_1} \gamma_l^2 + \sum_{l=1}^{L_2} \lambda_l^2\right). \quad (12)$$

The penalty p on the sum of the squared annotation parameters is the one used in ridge regression⁵⁰. In ridge regression, parameter estimates under this penalty are equivalent to estimating the posterior mean of the parameter if the prior distribution of the parameter is Gaussian⁵⁰; changing

the tuning parameter p is equivalent to changing the prior. We suspect that the interpretation in this model is similar. Since this penalized likelihood can not be used for formal statistical tests, we tune the p parameter by cross-validation. An alternative approach here would be to explicitly put a prior on the enrichment parameters, but in the absence of a conjugate prior this would likely add substantially to the computational burden for little practical benefit.

Cross-validation

To compare models and tune the penalty p in the penalized likelihood above, we used a 10-fold cross-validation approach. We split the chromosomal segments into 10 folds. Let θ_{-f}^p be the parameters of the model estimated while holding out the data from fold f and under penalty p , and $l_f^*(\theta_{-f}^p)$ be the penalized log-likelihood of the data in fold f under the model optimized without using fold f . Then:

$$l'(\theta^p) = \frac{1}{10} \sum_{i=1}^{10} l_i^*(\theta_{-i}^p). \quad (13)$$

Note that the size of the folds used in this cross-validation means that each fold excludes more than an entire chromosome. This means that no individual chromosome can have undue influence on the parameters included in the model.

Model choice

Consider a single phenotype and a set of L functional annotations of SNPs (in our case L is in the hundreds). Including all L SNP annotations in the model is neither biologically interesting nor computationally feasible. We thus set out to choose a relatively sparse model that fits the data. We start with forward selection: for each of the L annotations, we fit a model including a region-level parameter for regions in the top third of the distribution of gene density, a region-level parameter for regions in the bottom third of the distribution of gene density, a SNP-level parameter for SNPs from 0-5 kb from a TSS, a SNP-level parameter for SNPs from 5-10kb from a TSS, and a SNP-level parameter for the annotation in question. We then identify the set of annotations that significantly improve the model fit (as judged by the likelihood from Equation 10). We then:

1. Add the annotation that most significantly improves the likelihood to the model.
2. For each annotation identified as having a significant marginal effect, test a model including the annotation and those that have already been added.
3. If any annotation remains significant, go back to step 1.

At this point, there are generally a small number of annotations in the model, but the model may be over-fit. We then switch to using the 10-fold cross-validation likelihood in Equation 13. We first tune the penalty parameter p by finding the value of p that maximizes the cross-validation likelihood. We then:

1. Drop each annotation from the model in turn, and evaluate the cross-validation likelihood. When dropping annotations, we additionally try dropping the region-level annotations on gene density and the SNP-level annotations on distance to the nearest TSS.
2. If a simpler model has a higher cross-validation likelihood than the full model, drop the annotation from the model and return to step 1.
3. Report the model that has the highest cross-validation likelihood.

Approximating V_i

In order to compute the Bayes factor in Equation 4, we need an estimate of V_i , the standard error of the estimated effect size of SNP i . In principle, this is trivial output from standard regression software; however, it is rarely reported. Instead, let f_i be the minor allele frequency of SNP i computed from an external sample of the same ancestry as the population in which the association study was done (we use data from the 1000 Genomes Project³⁸). Let N_i be the number of individuals in the association study at SNP i (this can vary across SNPs due to missing data). Then:

$$V_i \approx \frac{1}{N_i f_i (1 - f_i)}. \quad (14)$$

Note that this variance is independent of the actual scale of the measurements; this is appropriate because the Z-scores are independent of the scale of the measurements as well.

Case-control studies

For all of the above, we have considered studies of quantitative traits. For a case-control study, we assume that we have summary statistics from logistic regression instead of linear regression. All aspects of the model are identical, with the exception of the approximation of V_i . Define N_{case} and $N_{control}$ as the numbers of cases and controls, respectively. Now,⁴⁹:

$$V_i \approx \frac{N_{case} + N_{control}}{N_{case} N_{control} [2f_i(1 - f_i) + 4f_i^2 - (2f_i(1 - f_i) + 4f_i^2)^2]}. \quad (15)$$

The variance here is on a log-odds scale.

Posterior probabilities of association

Once the model has been fit, we have empirical estimates of the prior probability that region k contains an association, $\hat{\Pi}_k$ and the prior probability that SNP i is the causal one, $\hat{\pi}_{ik}$ (conditional on there being an association). We define a Bayes factor summarizing the evidence for association in the *region* (see, for example Maller et al.⁴⁸):

$$BF_k^R = \sum_{i \in S_k} \hat{\pi}_{ik} BF_i, \quad (16)$$

where S_k is the set of SNPs in region k and BF_i is the Bayes factor for SNP i (Equation 4). The posterior probability that region k contains an association is then:

$$PPA_k^R = \frac{\hat{\Pi}_k BF_k^R / (1 - \hat{\Pi}_k)}{1 + \hat{\Pi}_k BF_k^R / (1 - \hat{\Pi}_k)} \quad (17)$$

We can also define the posterior probability that any given SNP i in region k is the causal one under our model:

$$PPA_{ik} = \frac{\hat{\pi}_{ik} BF_i}{\sum_{j \in S_k} \hat{\pi}_{jk} BF_j}. \quad (18)$$

This is similar to the calculation in Maller et al.⁴⁸, except that we allow the prior probability π_{ik} to vary across SNPs.

Finally, we can define the posterior probability that any given SNP is causal. This is the posterior probability that the region contains a causal SNP times the posterior probability that the SNP is causal conditional on there being an association in the region. If SNP i falls in region k :

$$PPA_i = PPA_k^R PPA_{ik}. \quad (19)$$

Conditional analysis

Because many of the annotations we consider are correlated, those ultimately included in the combined model for each trait (Figure 4) may be representatives of a large group of correlated annotations. For biological interpretation of the model, it is thus important to know which of the other annotations are interchangeable with those included in the model.

To test this, we took an approach of conditional analysis. Consider two SNP-level annotations, with annotation parameters λ_1 and λ_2 , respectively. In a joint model, we would jointly estimate both λ_1 and λ_2 . However, we are interested in whether the second annotation adds information above and beyond that provided by the first annotation. We thus first estimate λ_1 , then *fix* this parameter to its maximum likelihood value $\hat{\lambda}_1$. We then estimate $\lambda_2 | \hat{\lambda}_1$ – that is, we obtain the maximum likelihood estimate and 95% confidence interval of λ_2 *conditional* on a fixed value of λ_1 . If this confidence interval does not overlap zero, this is evidence that the second annotation adds information to the model above that provided by the first.

In practice, we first fit the combined model as described in the section “Model choice” above. We then returned to the set of annotations that had significant marginal associations. For each annotation in the combined model, we took each of the other annotations in turn and tested whether the included annotation was significantly more informative than the non-included annotation. In Figure 4 and Supplementary Figure 12, we display the total number of annotations represented by each one that is included in the combined model.

Acknowledgements. We thank David Reich, Nick Patterson, Alkes Price, and Po-Ru Loh for helpful discussions and suggestions; and Jonathan Pritchard, Graham Coop, and two anonymous reviewers for comments on a previous version of this manuscript. We thank Nicole Soranzo for providing access to the platelet studies, and Luke Jostins for assistance in obtaining the Crohn’s disease data. This work was supported by NIH postdoctoral fellowship GM103098 to JKP.

References

- [1] Visscher, P. M., Brown, M. A., McCarthy, M. I., and Yang, J. (2012). Five years of GWAS discovery. *Am J Hum Genet* *90*, 7–24.
- [2] Hindorff, L. A., Sethupathy, P., Junkins, H. A., Ramos, E. M., Mehta, J. P., Collins, F. S., and Manolio, T. A. (2009). Potential etiologic and functional implications of genome-wide association loci for human diseases and traits. *Proc Natl Acad Sci U S A* *106*, 9362–7.
- [3] ENCODE Project Consortium, Bernstein, B. E., Birney, E., Dunham, I., Green, E. D., Gunter, C., and Snyder, M. (2012). An integrated encyclopedia of DNA elements in the human genome. *Nature* *489*, 57–74.
- [4] Schork, A. J., Thompson, W. K., Pham, P., Torkamani, A., Roddey, J. C., Sullivan, P. F., Kelsoe, J. R., O’Donovan, M. C., Furberg, H., Tobacco and Genetics Consortium, et al. (2013). All SNPs are not created equal: genome-wide association studies reveal a consistent pattern of enrichment among functionally annotated SNPs. *PLoS Genet* *9*, e1003449.
- [5] Nicolae, D. L., Gamazon, E., Zhang, W., Duan, S., Dolan, M. E., and Cox, N. J. (2010). Trait-associated SNPs are more likely to be eQTLs: annotation to enhance discovery from gwas. *PLoS Genet* *6*, e1000888.
- [6] Lappalainen, T., Sammeth, M., Friedländer, M. R., ’t Hoen, P. A. C., Monlong, J., Rivas, M. A., González-Porta, M., Kurbatova, N., Griebel, T., Ferreira, P. G., et al. (2013). Transcriptome and genome sequencing uncovers functional variation in humans. *Nature* *501*, 506–11.
- [7] Cowper-Salari, R., Zhang, X., Wright, J. B., Bailey, S. D., Cole, M. D., Eeckhoutte, J., Moore, J. H., and Lupien, M. (2012). Breast cancer risk-associated SNPs modulate the affinity of chromatin for FOXA1 and alter gene expression. *Nat Genet* *44*, 1191–8.
- [8] Gerasimova, A., Chavez, L., Li, B., Seumois, G., Greenbaum, J., Rao, A., Vijayanand, P., and Peters, B. (2013). Predicting cell types and genetic variations contributing to disease by combining GWAS and epigenetic data. *PLoS One* *8*, e54359.
- [9] Trynka, G., Sandor, C., Han, B., Xu, H., Stranger, B. E., Liu, X. S., and Raychaudhuri, S. (2013). Chromatin marks identify critical cell types for fine mapping complex trait variants. *Nat Genet* *45*, 124–30.

- [10] Ernst, J., Kheradpour, P., Mikkelson, T. S., Shores, N., Ward, L. D., Epstein, C. B., Zhang, X., Wang, L., Issner, R., Coyne, M., et al. (2011). Mapping and analysis of chromatin state dynamics in nine human cell types. *Nature* *473*, 43–9.
- [11] Maurano, M. T., Humbert, R., Rynes, E., Thurman, R. E., Haugen, E., Wang, H., Reynolds, A. P., Sandstrom, R., Qu, H., Brody, J., et al. (2012). Systematic localization of common disease-associated variation in regulatory DNA. *Science* *337*, 1190–5.
- [12] Karczewski, K. J., Dudley, J. T., Kukurba, K. R., Chen, R., Butte, A. J., Montgomery, S. B., and Snyder, M. (2013). Systematic functional regulatory assessment of disease-associated variants. *Proceedings of the National Academy of Sciences* *110*, 9607–9612.
- [13] Paul, D. S., Nisbet, J. P., Yang, T.-P., Meacham, S., Rendon, A., Hautaviita, K., Tallila, J., White, J., Tijssen, M. R., Sivapalaratnam, S., et al. (2011). Maps of open chromatin guide the functional follow-up of genome-wide association signals: application to hematological traits. *PLoS Genet* *7*, e1002139.
- [14] Paul, D. S., Albers, C. A., Rendon, A., Voss, K., Stephens, J., HaemGen Consortium, van der Harst, P., Chambers, J. C., Soranzo, N., Ouwehand, W. H., et al. (2013). Maps of open chromatin highlight cell type-restricted patterns of regulatory sequence variation at hematological trait loci. *Genome Res* *23*, 1130–41.
- [15] van der Harst, P., Zhang, W., Leach, I. M., Rendon, A., Verweij, N., Sehmi, J., Paul, D. S., Elling, U., Allayee, H., Li, X., et al. (2012). Seventy-five genetic loci influencing the human red blood cell. *Nature* *492*, 369–375.
- [16] Parker, S. C. J., Stitzel, M. L., Taylor, D. L., Orozco, J. M., Erdos, M. R., Akiyama, J. A., van Bueren, K. L., Chines, P. S., Narisu, N., NISC Comparative Sequencing Program, et al. (2013). Chromatin stretch enhancer states drive cell-specific gene regulation and harbor human disease risk variants. *Proc Natl Acad Sci U S A*.
- [17] Global Lipids Genetics Consortium, Willer, C. J., Schmidt, E. M., Sengupta, S., Peloso, G. M., Gustafsson, S., Kanoni, S., Ganna, A., Chen, J., Buchkovich, M. L., et al. (2013). Discovery and refinement of loci associated with lipid levels. *Nat Genet* *45*, 1274–83.
- [18] Hnisz, D., Abraham, B. J., Lee, T. I., Lau, A., Saint-André, V., Sigova, A. A., Hoke, H. A., and Young, R. A. (2013). Super-enhancers in the control of cell identity and disease. *Cell*.
- [19] Lui, J. C., Nilsson, O., Chan, Y., Palmer, C. D., Andrade, A. C., Hirschhorn, J. N., and Baron, J. (2012). Synthesizing genome-wide association studies and expression microarray reveals novel genes that act in the human growth plate to modulate height. *Hum Mol Genet* *21*, 5193–201.

- [20] Hu, X., Kim, H., Stahl, E., Plenge, R., Daly, M., and Raychaudhuri, S. (2011). Integrating autoimmune risk loci with gene-expression data identifies specific pathogenic immune cell subsets. *The American Journal of Human Genetics* *89*, 496–506.
- [21] Kindt, A. S. D., Navarro, P., Semple, C. A. M., and Haley, C. S. (2013). The genomic signature of trait-associated variants. *BMC Genomics* *14*, 108.
- [22] Gagliano, S. A., Barnes, M. R., Weale, M. E., and Knight, J. (2013). A Bayesian method to incorporate hundreds of functional characteristics with association evidence to improve variant prioritization. *bioRxiv*.
- [23] Veyrieras, J.-B., Kudaravalli, S., Kim, S. Y., Dermitzakis, E. T., Gilad, Y., Stephens, M., and Pritchard, J. K. (2008). High-resolution mapping of expression-QTLs yields insight into human gene regulation. *PLoS Genet* *4*, e1000214.
- [24] Gaffney, D. J., Veyrieras, J.-B., Degner, J. F., Pique-Regi, R., Pai, A. A., Crawford, G. E., Stephens, M., Gilad, Y., and Pritchard, J. K. (2012). Dissecting the regulatory architecture of gene expression QTLs. *Genome Biol* *13*, R7.
- [25] Lee, S.-I., Dudley, A. M., Drubin, D., Silver, P. A., Krogan, N. J., Pe’er, D., and Koller, D. (2009). Learning a prior on regulatory potential from eQTL data. *PLoS Genet* *5*, e1000358.
- [26] Lango-Allen, H., Estrada, K., Lettre, G., Berndt, S. I., Weedon, M. N., Rivadeneira, F., Willer, C. J., Jackson, A. U., Vedantam, S., Raychaudhuri, S., et al. (2010). Hundreds of variants clustered in genomic loci and biological pathways affect human height. *Nature* *467*, 832–838.
- [27] Teslovich, T. M., Musunuru, K., Smith, A. V., Edmondson, A. C., Stylianou, I. M., Koseki, M., Pirruccello, J. P., Ripatti, S., Chasman, D. I., Willer, C. J., et al. (2010). Biological, clinical and population relevance of 95 loci for blood lipids. *Nature* *466*, 707–713.
- [28] Lewinger, J. P., Conti, D. V., Baurley, J. W., Triche, T. J., and Thomas, D. C. (2007). Hierarchical Bayes prioritization of marker associations from a genome-wide association scan for further investigation. *Genet Epidemiol* *31*, 871–82.
- [29] Heron, E. A., O’Dushlaine, C., Segurado, R., Gallagher, L., and Gill, M. (2011). Exploration of empirical Bayes hierarchical modeling for the analysis of genome-wide association study data. *Biostatistics* *12*, 445–461.
- [30] Chen, G. K. and Witte, J. S. (2007). Enriching the analysis of genomewide association studies with hierarchical modeling. *Am J Hum Genet* *81*, 397–404.
- [31] Carbonetto, P. and Stephens, M. (2013). Integrated enrichment analysis of variants and pathways in genome-wide association studies indicates central role for IL-2 signaling genes in type 1 diabetes, and cytokine signaling genes in Crohn’s disease. *PLoS Genet* *9*, e1003770.

- [32] Gieger, C., Radhakrishnan, A., Cvejic, A., Tang, W., Porcu, E., Pistis, G., Serbanovic-Canic, J., Elling, U., Goodall, A. H., Labrune, Y., et al. (2011). New gene functions in megakaryopoiesis and platelet formation. *Nature* *480*, 201–208.
- [33] Jostins, L., Ripke, S., Weersma, R. K., Duerr, R. H., McGovern, D. P., Hui, K. Y., Lee, J. C., Schumm, L. P., Sharma, Y., Anderson, C. A., et al. (2012). Host-microbe interactions have shaped the genetic architecture of inflammatory bowel disease. *Nature* *491*, 119–124.
- [34] Speliotes, E. K., Willer, C. J., Berndt, S. I., Monda, K. L., Thorleifsson, G., Jackson, A. U., Allen, H. L., Lindgren, C. M., Luan, J., Mägi, R., et al. (2010). Association analyses of 249,796 individuals reveal 18 new loci associated with body mass index. *Nature genetics* *42*, 937–948.
- [35] Estrada, K., Styrkarsdottir, U., Evangelou, E., Hsu, Y.-H., Duncan, E. L., Ntzani, E. E., Oei, L., Albagha, O. M., Amin, N., Kemp, J. P., et al. (2012). Genome-wide meta-analysis identifies 56 bone mineral density loci and reveals 14 loci associated with risk of fracture. *Nature genetics* *44*, 491–501.
- [36] Manning, A. K., Hivert, M.-F., Scott, R. A., Grimsby, J. L., Bouatia-Naji, N., Chen, H., Rybin, D., Liu, C.-T., Bielak, L. F., Prokopenko, I., et al. (2012). A genome-wide approach accounting for body mass index identifies genetic variants influencing fasting glycemic traits and insulin resistance. *Nature genetics* *44*, 659–669.
- [37] Pasaniuc, B., Zaitlen, N., Shi, H., Bhatia, G., Gusev, A., Pickrell, J., Hirschhorn, J., Strachan, D. P., Patterson, N., and Price, A. L. (2013). Fast and accurate imputation of summary statistics enhances evidence of functional enrichment. arXiv preprint arXiv:1309.3258.
- [38] Abecasis, G., Altshuler, D., Auton, A., Brooks, L., Durbin, R., Gibbs, R. A., Hurles, M. E., McVean, G. A., Bentley, D., Chakravarti, A., et al. (2010). A map of human genome variation from population-scale sequencing. *Nature* *467*, 1061–1073.
- [39] Thurman, R. E., Rynes, E., Humbert, R., Vierstra, J., Maurano, M. T., Haugen, E., Sheffield, N. C., Stergachis, A. B., Wang, H., Vernot, B., et al. (2012). The accessible chromatin landscape of the human genome. *Nature* *489*, 75–82.
- [40] Hoffman, M. M., Ernst, J., Wilder, S. P., Kundaje, A., Harris, R. S., Libbrecht, M., Giardine, B., Ellenbogen, P. M., Bilmes, J. A., Birney, E., et al. (2013). Integrative annotation of chromatin elements from ENCODE data. *Nucleic acids research* *41*, 827–841.
- [41] Stephens, M. (2013). A unified framework for association analysis with multiple related phenotypes. *PLoS One* *8*, e65245.
- [42] Deutsch, V. R. and Tomer, A. (2006). Megakaryocyte development and platelet production. *Br J Haematol* *134*, 453–66.

- [43] Giambartolomei, C., Vukcevic, D., Schadt, E. E., Hingorani, A. D., Wallace, C., and Plagnol, V. (2013). Bayesian test for co-localisation between pairs of genetic association studies using summary statistics. arXiv preprint arXiv:1305.4022.
- [44] Degner, J. F., Pai, A. A., Pique-Regi, R., Veyrieras, J.-B., Gaffney, D. J., Pickrell, J. K., De Leon, S., Michelini, K., Lewellen, N., Crawford, G. E., et al. (2012). DNaseI sensitivity QTLs are a major determinant of human expression variation. *Nature* *482*, 390–4.
- [45] Plagnol, V., Smyth, D. J., Todd, J. A., and Clayton, D. G. (2009). Statistical independence of the colocalized association signals for type 1 diabetes and RPS26 gene expression on chromosome 12q13. *Biostatistics* *10*, 327–34.
- [46] Nica, A. C., Montgomery, S. B., Dimas, A. S., Stranger, B. E., Beazley, C., Barroso, I., and Dermitzakis, E. T. (2010). Candidate causal regulatory effects by integration of expression QTLs with complex trait genetic associations. *PLoS Genet* *6*, e1000895.
- [47] Yang, J., Ferreira, T., Morris, A. P., Medland, S. E., Genetic Investigation of ANthropometric Traits (GIANT) Consortium, DIAbetes Genetics Replication And Meta-analysis (DIAGRAM) Consortium, Madden, P. A. F., Heath, A. C., Martin, N. G., Montgomery, G. W., et al. (2012). Conditional and joint multiple-SNP analysis of GWAS summary statistics identifies additional variants influencing complex traits. *Nat Genet* *44*, 369–75, S1–3.
- [48] Maller, J. B., McVean, G., Byrnes, J., Vukcevic, D., Palin, K., Su, Z., Howson, J. M., Auton, A., Myers, S., Morris, A., et al. (2012). Bayesian refinement of association signals for 14 loci in 3 common diseases. *Nature genetics* *44*, 1294–1301.
- [49] Wakefield, J. (2008). Bayes factors for genome-wide association studies: comparison with p-values. *Genet Epidemiol* *33*, 79–86.
- [50] Hastie, T., Tibshirani, R., and Friedman, J. J. H. (2001). *The elements of statistical learning* volume 1. (Springer New York).

Supplementary material for: Joint analysis of functional genomic
data and genome-wide association studies of 18 human traits

Joseph K. Pickrell^{1,2}

¹ New York Genome Center, New York, NY

² Department of Biological Sciences, Columbia University, New York, NY

Correspondence to: jkpickrell@nygenome.org

June 16, 2022

Contents

1	GWAS data	2
1.1	GIANT data	2
1.2	GEFOS data	2
1.3	IIBDGC data	2
1.4	MAGIC data	2
1.5	Global lipid genetics consortium data	3
1.6	Red blood cell trait data	3
1.7	Platelet traits	3
2	Functional genomic data	4
2.1	DNase-I hypersensitivity data	4
2.2	Chromatin state data	4
2.3	Gene models	5
3	Imputation of summary statistics	5
4	Details of application of the hierarchical model	5
4.1	Simulations	5
4.2	Robustness to choice of prior and window size	6
4.3	Quantifying the relative roles of coding versus non-coding changes in each phenotype	6
4.4	Interaction effects in annotation models	7
4.5	Calibrating a “significance” threshold	7
4.6	Identification of novel loci	8

1 GWAS data

1.1 GIANT data

We downloaded summary statistics from large GWAS of height [Lango-Allen et al., 2010] and BMI [Speliotes et al., 2010] from http://www.broadinstitute.org/collaboration/giant/index.php/GIANT_consortium. The height summary statistics consisted of 2,469,635 SNPs either directly genotyped or imputed in an average of 129,945 individuals. We removed all SNPs with a sample size of less than 120,000 individuals. The BMI summary statistics consisted of 2,471,516 summary statistics either directly genotyped or imputed in an average of 120,569 individuals. We removed all SNPs with a sample size of less than 110,000 individuals. We then imputed summary statistics at SNPs identified in the 1000 Genomes Project as described in Section 3.

1.2 GEFOS data

We downloaded summary statistics from large GWAS of bone mineral density [Estrada et al., 2012] from <http://www.gefos.org/?q=content/data-release>. There are two traits in these data: bone density measured in the femoral neck and bone density measured in the lumbar spine. The femoral neck bone density GWAS consisted of 2,478,337 SNPs, and the lumbar spine bone density consisted of 2,468,080 SNPs. Because the sample size at each SNP was not reported, we used the overall study sample sizes of 32,961 and 31,800 as approximations of the sample size at each SNP, and imputed summary statistics as described in Section 3.

1.3 IIBDGC data

We downloaded summary statistics from a large GWAS of Crohn's disease [Jostins et al., 2012] from <http://www.ibdgenetics.org/downloads.html>. The downloaded data consisted of 953,242 SNPs. Because the sample size at each SNP was not reported, we used the overall study sample sizes of 6,299 cases and 15,148 controls as approximations of the sample size at each SNP, and imputed summary statistics as described in Section 3. Note that summary statistics from a GWAS of ulcerative colitis were also available from this site; however, these data contain a number of false positive associations that were filtered by Jostins et al. [2012] using criteria that were not available to us. We thus only used the Crohn's disease association study.

1.4 MAGIC data

We downloaded summary statistics from a large GWAS of fasting glucose levels [Manning et al., 2012] from <http://www.magicinvestigators.org/downloads/>. The downloaded data consisted of 2,628,880 SNPs. Because the sample size at each SNP was not reported, we used the overall study sample size of 58,074 as an approximation of the sample size at each SNP, and imputed summary statistics as described in Section 3.

1.5 Global lipid genetics consortium data

We downloaded summary statistics from a large GWAS of lipid traits [Teslovich et al., 2010] from <http://www.sph.umich.edu/csg/abecasis/public/lipids2010/>. These data consist of summary statistics for association studies of four traits: LDL cholesterol, HDL cholesterol, triglycerides, and total cholesterol. The HDL data consisted of 2,692,429 SNPs genotyped or imputed in an average of 88,754 individuals, the LDL data consisted of 2,692,564 SNPs genotyped or imputed in an average of 84,685 individuals, the total cholesterol data consisted of 2,692,413 SNPs genotyped or imputed in an average of 89,005 individuals, and the triglycerides data consisted of 2,692,560 SNPs genotypes or imputed in an average of 85,691 individuals. For all traits, we removed SNPs with a sample size less than 80,000 individuals, and imputed summary statistics as described in Section 3.

To calibrate significance thresholds, we additionally used summary statistics from Global Lipids Genetics Consortium et al. [2013]. These were downloaded from <http://www.sph.umich.edu/csg/abecasis/public/lipids2013/>.

1.6 Red blood cell trait data

We obtained summary statistics from a large GWAS of red blood cell traits [van der Harst et al., 2012] from the European Genome-Phenome Archive (accession number EGAS00000000132). We downloaded summary statistics from association studies of six traits: hemoglobin levels, mean cell hemoglobin (MCH), mean corpuscular hemoglobin concentration (MCHC), mean cell volume (MCV), packed cell volume (PCV), and red blood cell count (RBC). The hemoglobin level data consisted of 2,593,078 SNPs genotyped or imputed in 50,709 individuals, the MCH data consisted of 2,586,785 SNPs genotyped or imputed in an average of 43,127 individuals, the MCHC data consisted of 2,588,875 SNPs genotyped or imputed in an average of 46,469 individuals, the MCV data consisted of 2,591,132 SNPs genotyped or imputed in an average of 47,965 individuals, the PCV data consisted of 2,591,079 SNPs genotyped or imputed in an average of 44,485 individuals, and the RBC data consisted of 2,589,454 SNPs genotyped or imputed in an average of 44,851 individuals. We removed all SNPs with a sample size of less than 50,000 individuals (for hemoglobin levels) or 40,000 individuals (for the other traits), and imputed summary statistics as described in Section 3.

1.7 Platelet traits

Summary statistics from a large GWAS of platelet traits [Gieger et al., 2011] were generously provided to us by Nicole Soranzo. The data consist of summary statistics from association studies of two traits: platelet counts and mean platelet volume. The platelet count data consisted of 2,705,636 SNPs genotyped or imputed in an average of 44,217 individuals, and the platelet volume data consisted of 2,690,858 SNPs genotyped or imputed in an average of 16,745 individuals. We removed all SNPs with sample sizes less than 40,000 (for platelet counts) or 15,000 (for platelet volume), and imputed summary statistics as described in Section 3.

2 Functional genomic data

2.1 DNase-I hypersensitivity data

We downloaded DNase-I hypersensitivity data from two sources. The first was a set of regions defined as DNase-I hypersensitive by Maurano et al. [2012] in 349 samples. We downloaded .bed files for 349 samples from http://www.uwencode.org/proj/Science_Maurano_Humbert_et_al/ on February 13, 2013. These samples include 116 samples from cell lines or sorted blood cells, and 333 samples from primary fetal tissues. These latter samples were sampled from several tissues at various time points; we treated each track as independent rather than pooling data from tissues, since different experiments may have slightly different properties. The tissues in this latter group are fetal heart, fetal brain, fetal lung, fetal kidney, fetal intestine (large and small), fetal muscle, fetal placenta, and fetal skin.

The second was a set of regions defined as DNase-I hypersensitive by the Crawford lab in the context of the ENCODE project [Thurman et al., 2012]. We downloaded .bed files for 53 samples from http://ftp.ebi.ac.uk/pub/databases/ensembl/encode/integration_data_jan2011/byDataType/openchrom/jan2011/fdrPeaks/ on March 29, 2013. We restricted ourselves to the files labeled as being generated at Duke University. Each experiment defined a set of regions of open chromatin in a particular cell type or cell line.

The “Duke” DNase-I hypersensitive sites are all of exactly 150 bases in length, and each annotation covers approximately 1% of the genome (range: 0.4 - 1.9 % of the genome). The “Maurano” DNase-I hypersensitive sites are on average 514 bases long, and each covers on average 2.7% of the genome (range: 0.9-5.1 % of the genome).

2.2 Chromatin state data

We downloaded the “genome segmentations” of the six ENCODE cell lines [Hoffman et al., 2013] from http://ftp.ebi.ac.uk/pub/databases/ensembl/encode/integration_data_jan2011/byDataType/segmentations/jan2011/hub/ on December 18, 2012. We used the “combined” segmentation from two algorithms. This segmentation splits the genome into non-overlapping regions described as CTCF binding sites, enhancers, promoter-flanking regions, repressed chromatin, transcribed regions, transcription start sites, and weak enhancers. This segmentation was done independently in each of six cell lines, for a total of 42 annotations.

Overall the “repressed chromatin” mark covers the largest fraction of the genome, on average 66% (ranging from 60% for HUVEC cells to 70% for H1 ES cells). The “transcribed” mark covers on average 13% of the genome, the “CTCF” mark 1% of the genome, the “enhancer” mark 0.9% of the genome, the “TSS” mark 0.7% of the genome, the “weak enhancer” mark 0.4% of the genome, and the “promoter-flanking” mark 0.2% of the genome. The remainder of the genome is not mappable by short reads and it thus excluded from these annotations.

2.3 Gene models

We downloaded the Ensembl gene annotations from the UCSC genome browser on May 21. Annotations of nonsynonymous and synonymous status for all SNPs in phase 1 of the 1000 Genomes Project were obtained from `ftp://ftp-trace.ncbi.nih.gov/1000genomes/ftp/phase1/analysis_results/functional_annotation/annotated_vcfs/`. Coding exons cover about 3% of the genome, while 3' UTRs and 5' UTRs cover 2% and 0.6% of the genome, respectively.

3 Imputation of summary statistics

We used ImpG v1.0 [Pasaniuc et al., 2013] under the default settings to impute summary statistics from all GWAS. As a reference panel, we used all haplotypes from European individuals in phase 1 of the 1000 Genomes Project, and only used SNPs with a minor allele frequency greater than 2%. The reference haplotype files were derived from the 1000 Genomes integrated phase 1 v3.20101123 calls, downloaded from `ftp://ftp-trace.ncbi.nih.gov/1000genomes/ftp/phase1/analysis_results/integrated_call_sets/`. We used all 379 individuals labeled as “European”. After imputation, we removed all imputed SNPs with a predicted accuracy (in terms of correlation with the true summary statistics) less than 0.8. Overall, for each GWAS, we successfully imputed about 75-80% of SNPs with a minor allele frequency over 10% (Figure 1).

To verify that imputation did not induce inflation of the test statistics, we computed the genomic control inflation factor λ_{GC} [Bacanu et al., 2002] before and after imputation (Supplementary Table 1). In all studies, inflation decreased after imputation, sometimes leading to a marked deflation in the test statistics. This is consistent with previous observations using this software [Pasaniuc et al., 2013]. The reason for this deflation is the shrinkage prior used in the imputation, which leads to conservative estimates of significance (imposed to strictly avoid false positive associations).

4 Details of application of the hierarchical model

4.1 Simulations

To test the performance of the model, we performed simulations using a GWAS of height [Lango-Allen et al., 2010]. Using the imputed summary statistics, we split the genome into blocks of 5,000 SNPs, then extracted the blocks with a genome-wide significant SNP reported in Lango-Allen et al. [2010]. In each block, we had a reported Z-score for each SNP. To simulate annotations, we called the SNP with the smallest P-value in the region the “causal” SNP. We then simulated annotations by placing all non-“casual” SNPs in an annotation with rate r_1 , and all “casual” SNPs in the annotation with rate r_2 . We also varied the numbers of blocks included in the model. In each simulation, we randomly assigned SNPs to annotations according to determined rates, then ran our model under the assumption that $\Pi_k = 1$, that is, all blocks contain a causal SNP. We then calculated power as the fraction of simulations in which the confidence intervals of the annotation effect did not overlap zero.

We chose parameter settings of r_1 and r_2 such that the enrichment factors were similar to those in observed data (log-enrichment of 0.98 and 1.80). We chose r_1 to be either 0.2 and 0.1. For each set of parameters, we simulated 100 annotations and ran the model separately on each. Shown in Figure 2 is the power of the model. As expected, power increased as r_1 or the effect size increased, and as the number of loci increased.

4.2 Robustness to choice of prior and window size

There are two parameters in the model that are set by the user—the prior variance W on the effect size and the window size defining “independent” blocks of the genome. We empirically tested the robustness of the model to variation in these parameters using the Crohn’s disease dataset. We ran the model on each annotation using $W = 0.1$ and $W = 0.5$, additionally including—as in our main analyses—region-level parameters for regions in the top third and bottom third of gene density and SNP-level parameters for SNPs located from 0-5kb from a transcription start site and SNPs 5-10kb from a transcription start site. Plotted in Figure 16A are these annotation parameter estimates for all annotations where the 95% confidence intervals did not overlap 0 in at least one run. The estimates from the two runs with different priors are highly correlated. We additionally tested window sizes of 5,000 SNPs and 10,000 SNPs (both with $W = 0.1$). The annotation effect estimates from these two window sizes are plotted in Figure 16B, and again are highly correlated.

4.3 Quantifying the relative roles of coding versus non-coding changes in each phenotype

To generate Figure 3 in the main text, we fit a model to each GWAS where we included region-level annotations for regions in the top third and bottom third of the distribution of gene density, and SNP-level annotations for non-synonymous SNPs and SNPs within 5kb of a transcription start site. Shown in Figure 3A in the main text are the estimates of the enrichment parameter for non-synonymous SNPs. At each SNP, the result of this model is the posterior probability that the SNP is casual (see Equation 19 in the main text). If we let this posterior probability at SNP i be PPA_i , then the fraction of causal SNPs that are non-synonymous, f_{NS} is:

$$f_{NS} = \frac{\sum_i PPA_i I_i^{NS}}{\sum_i PPA_i}, \quad (1)$$

where I_i^{NS} is an indicator variable that takes value one if SNP i is non-synonymous and zero otherwise. To get error bars on this fraction, we performed a block jackknife. We split the genome into 20 blocks with equal numbers of SNPs. If f_{NS}^j is the estimate of the fraction of casual SNPs that are non-synonymous excluding block j , then:

$$SE = \sqrt{\frac{19}{20} \sum_{j=1}^{20} (f_{NS}^j - \bar{f}_{NS})^2}, \quad (2)$$

where $\bar{f}_{NS} = \frac{1}{20} \sum_{i=1}^{20} f_{NS}^i$. In Supplementary Figure 3, we show the corresponding results for synonymous SNPs.

4.4 Interaction effects in annotation models

As noted in the main text, there were two cases in which the sign of the annotation effect flipped between the single annotation models and the combined models. These were Crohn’s disease (Supplementary Table 6) and red blood cell count (Supplementary Table 18). In the main text we discuss the Crohn’s disease example. For the red blood cell count example, note that SNPs influencing this trait are enriched in the annotation of DNase-I hypersensitive sites in the fetal renal pelvis when this annotation is considered alone (\log_2 enrichment of 2.48, 95% CI [0.04, 4.17]). This annotation is correlated with the fetal stomach annotation, which has a \log_2 enrichment of 4.83 (95% CI [3.30, 6.45]) when treated alone. The SNPs in both of these annotations have a \log_2 enrichment of 2.41 (95% CI [-1.83, 4.23]), which leads to the interaction effect. Essentially the signal in the fetal stomach is driven by those SNPs that fall in DNase-I hypersensitive sites in the fetal stomach but *not* the fetal renal pelvis. This suggests that there are a subset of DNase-I hypersensitive sites that are of particular interest for this phenotype. The interpretation of the Crohn’s disease example is similar.

4.5 Calibrating a “significance” threshold

For each genomic region, our method estimates the posterior probability that the region contains a SNP associated with a trait. If the model were a perfect description of reality, this probability could be interpreted literally. Since the model is not perfect, however, we sought a more empirical calibration. We used the fact that we initially ran the method on the GWAS data reported by Teslovich et al. [2010] on four lipid traits. Since then, a GWAS with more individuals (though at a considerably smaller number of SNPs) has been reported for these four traits [Global Lipids Genetics Consortium et al., 2013]. This latter study contains many of the individuals from the former (which had approximately 90,000 individuals), as well as about 80,000 more individuals. However, the additional individuals were genotyped in the MetaboChip [Voight et al., 2012], which has less than 200,000 markers, rather than the more dense standard GWAS arrays. This means that some regions of the genome do not benefit from the larger sample size.

For each region of the genome for each of the four traits, we built a table containing the minimum P-value from Teslovich et al. [2010], the posterior probability of association in the region (computed using the data from Teslovich et al. [2010]), the minimum P-value from Global Lipids Genetics Consortium et al. [2013], and the sample size used to get this minimum P-value (from Global Lipids Genetics Consortium et al. [2013]). We discarded regions where sample size at the SNP with the minimum P-value in the replication data set was smaller than 120,000 (since in these regions there is essentially no new data). We then coded each region as a “true positive” if the minimum P-value from Global Lipids Genetics Consortium et al. [2013] was less than 5×10^{-8}

and a “true negative” otherwise. In Figure 15, we plot the number of “true positives” and “false negatives” that exceed various P-value and PPA thresholds. Note that since the data in Global Lipids Genetics Consortium et al. [2013] is not independent of that in Teslovich et al. [2010], this comparison is not appropriate for evaluating the relative performance of P-values versus the PPA. Our goal was simply to find a PPA threshold with similar performance in terms of reducing the number of false positives as the standard P-value threshold of 5×10^{-8} .

By visual inspection we set a PPA threshold at 0.9 (Figure 15). At this threshold, we identify 45 “true positives” and zero “false positives” for HDL, 43 and 1 for LDL, 47 and zero for total cholesterol, and 27 and zero for triglycerides. These are similar to the numbers for a P-value threshold of 5×10^{-8} (Supplementary Table 21). Combining the loci identified by both methods leads to 48 loci for HDL (versus 43 using a P-value threshold), 44 for LDL (versus 40), 51 for TC (versus 51) and 30 for TG (versus 29). This is on average an increase of 6% in the number of loci identified. Note that this number is likely a lower bound, since the P-values in the replication study are naturally highly correlated to those in the initial study since they use many of the same individuals. A proper comparison would use a completely separate, large set of individuals to determine “true positives” and “true negatives”, but such samples are not yet available.

4.6 Identification of novel loci

For each fitted model (using the parameters from Supplementary Tables 3-20 estimated using the penalized likelihood), we calculated the posterior probability of association in each genomic region. We then identified all regions with a PPA greater than 0.9 but that had a minimum P-value less than 5×10^{-8} . For each remaining region, we identified the “lead” SNP as the SNP with the largest posterior probability of being the causal SNP in the region. If this SNP was within 500kb of a SNP with $P < 5 \times 10^{-8}$ (this can happen because we use non-overlapping windows and sometimes the best SNP is at the edge of the region), we removed it. We also manually removed two regions (surrounding rs8076131 in Crohn’s disease and surrounding rs11535944 in HDL), where the “new” association was in LD with a previously reported SNP over 500kb away. In Supplementary Table 22, we show the remaining SNPs; these regions are high-confidence associations that did not reach traditional genome-wide significance.

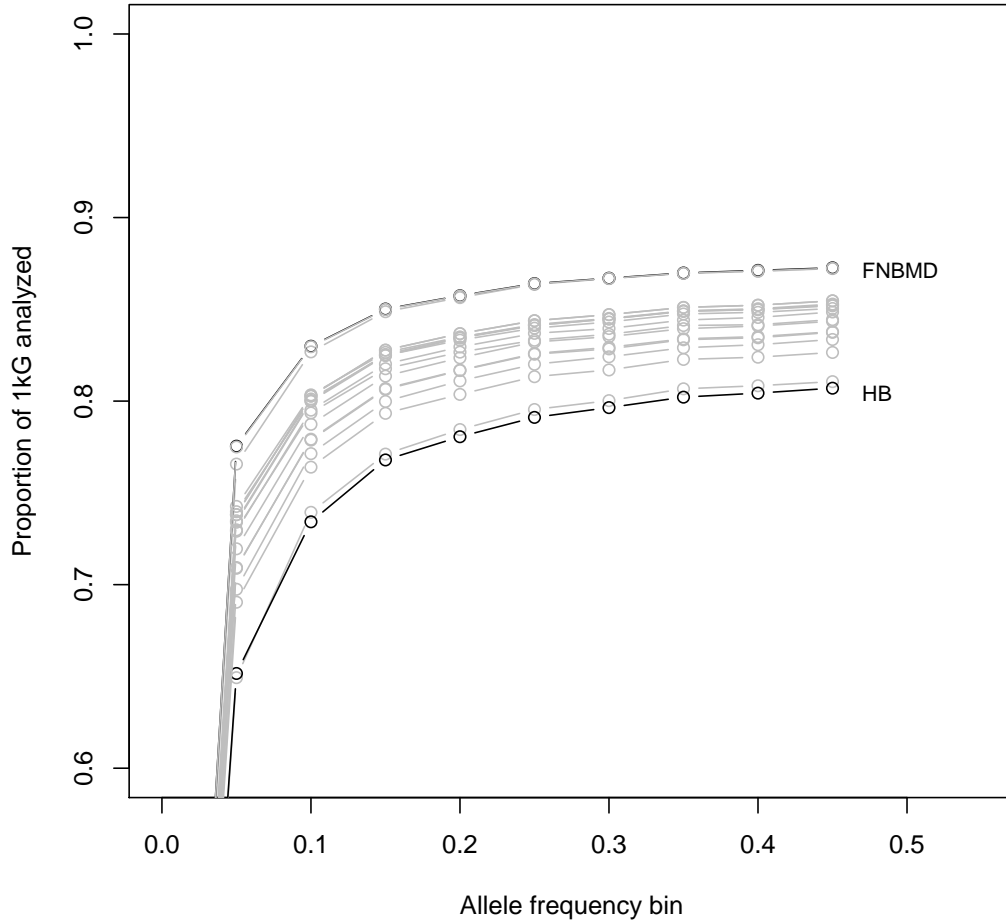


Figure 1. **Proportion of SNPs in the 1000 Genomes Project either genotyped or successfully imputed.** For each trait, we split all SNPs in phase 1 of the 1000 Genomes Project into bins based on their minor allele frequency in the European population. Bin sizes were of 5% frequency. Shown are the proportions of SNPs in each bin that were either genotyped or successfully imputed for each trait (the points are at the lower ends of the bins, such that the point at 45% frequency contains all SNPs from 45%-50% minor allele frequency). Labeled are the traits with the lowest and highest coverage. HB = hemoglobin levels, FNBMD = femoral neck bone mineral density.

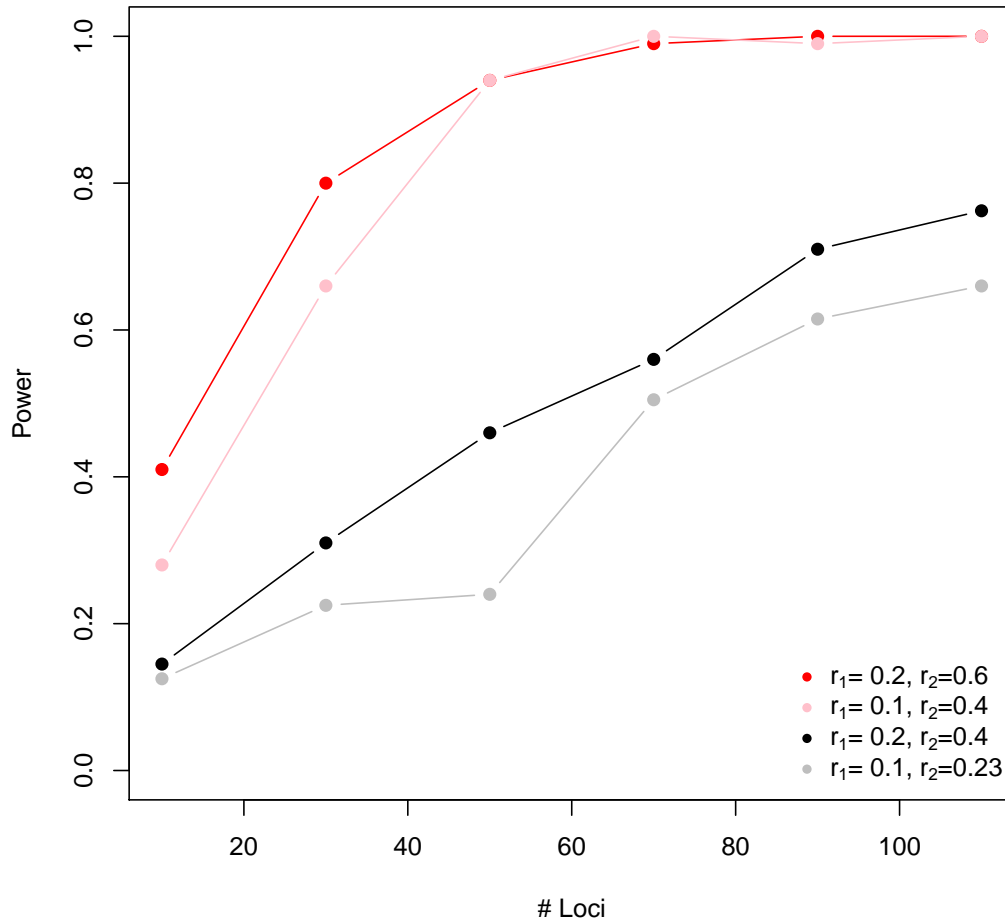
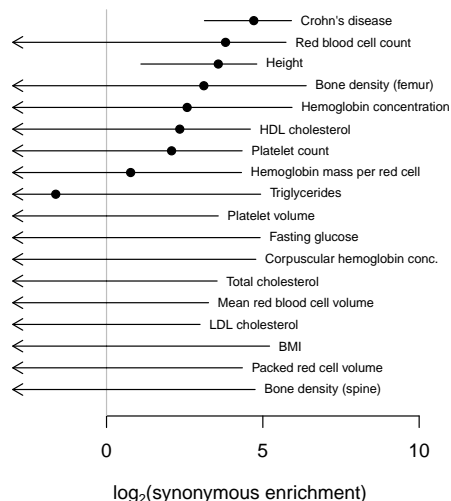


Figure 2. **Power to detect a significant annotation.** We simulated GWAS data under different levels of enrichment of causal SNPs in an annotation (see Supplementary Text), then evaluated the power of the method to detect the enrichment with different numbers of loci. In red and pink are log₂-enrichments of 2.6, and in black and grey are log₂-enrichments of 1.4.

A. Enrichment of synonymous SNPs among GWAS hits



B. Proportion of associated SNPs that are synonymous

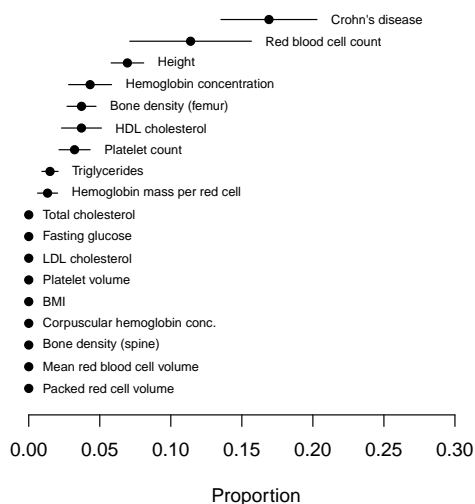


Figure 3. **Estimated role of synonymous polymorphisms in each trait.** **A. Estimated enrichment of synonymous SNPs.** For each trait, we fit a model including an effect of synonymous SNPs and an effect of SNPs within 5kb of a TSS. Shown are the estimated enrichment parameters and 95% confidence intervals for the synonymous SNPs. **B. Estimated proportion of GWAS hits driven by synonymous SNPs.** For each trait, using the model fit in A., we estimated the proportion of GWAS signals driven by synonymous SNPs. Shown is this estimate and its standard error.

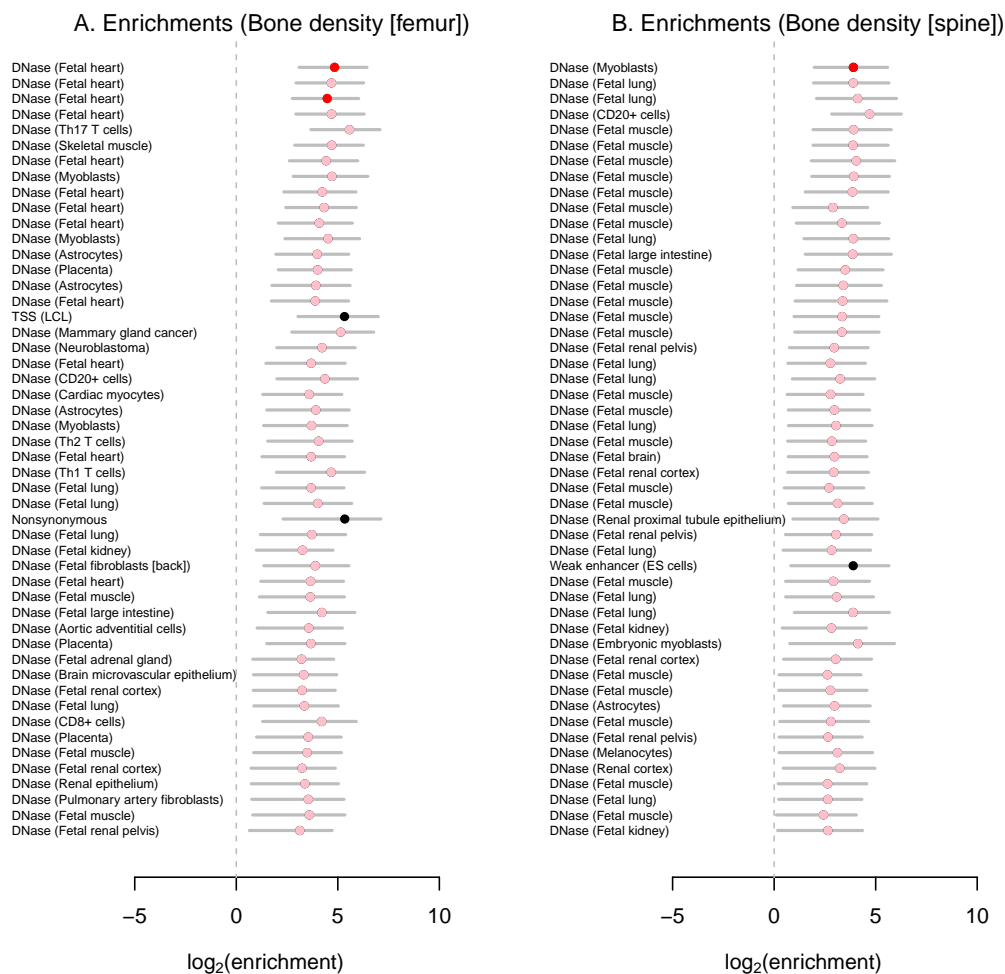


Figure 4. **Annotation effects in the bone mineral density data.** We estimated an enrichment parameter for each annotation individually in the GWAS for **A.** bone density in the femoral neck and **B.** bone density in the lumbar spine. Shown are the maximum likelihood estimates and 95% confidence intervals. Annotations are ranked according to how much each improves the fit of the model; shown are the 50 annotations that most improve the model (or if there were less than 50 significant annotations, all of the significant annotations). In red are the annotations included in the combined model, and in pink are annotations that are statistically equivalent to those in the combined model.

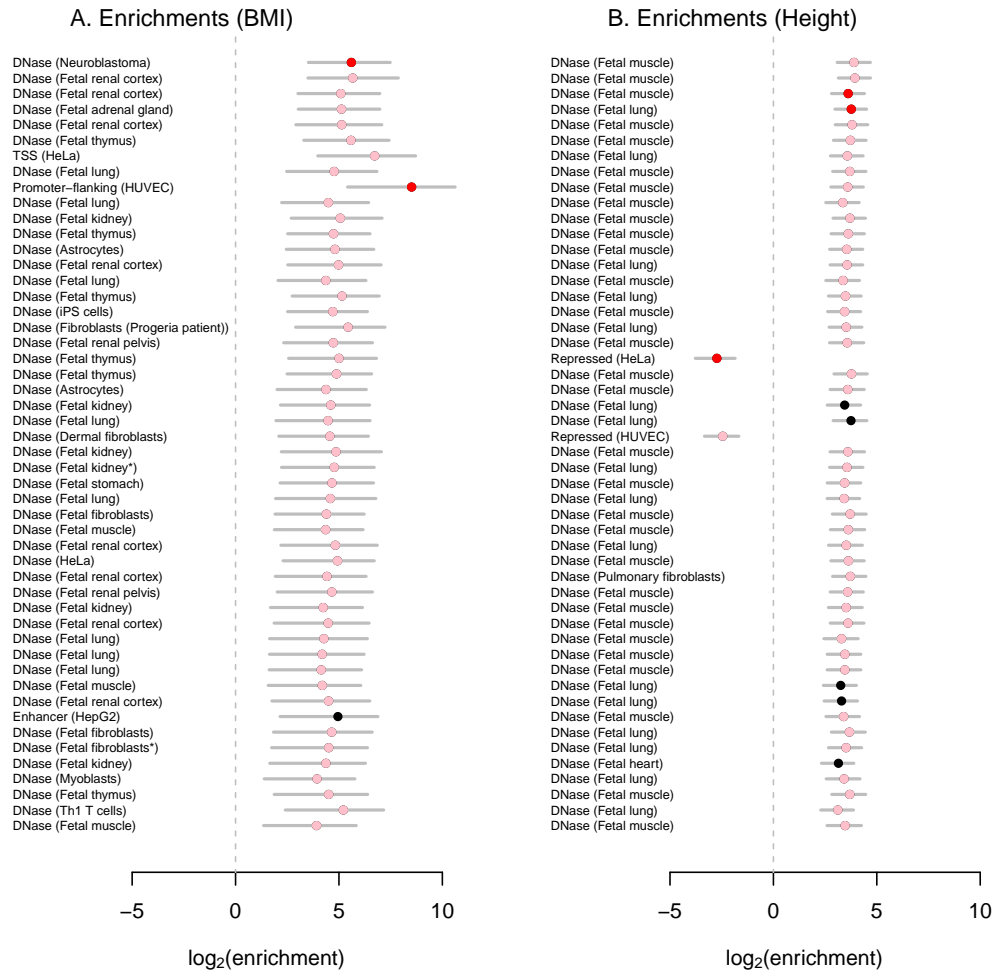


Figure 5. **Annotation effects in the GIANT data.** We estimated an enrichment parameter for each annotation individually in the GWAS for **A.** BMI and **B.** height. Shown are the maximum likelihood estimates and 95% confidence intervals. Annotations are ranked according to how much each improves the fit of the model; shown are the 50 annotations that most improve the model (or if there were less than 50 significant annotations, all of the significant annotations). In red are the annotations included in the combined model, and in pink are annotations that are statistically equivalent to those in the combined model.

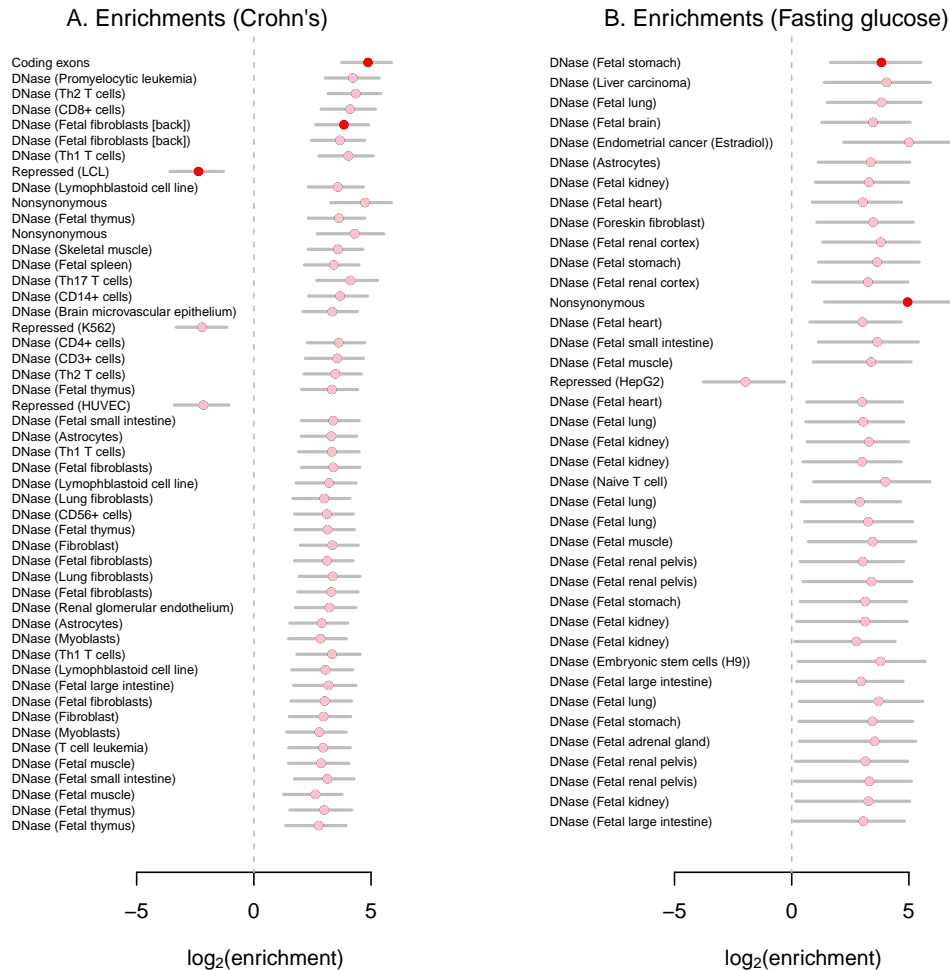


Figure 6. **Annotation effects in the Crohn's disease and fasting glucose data.** We estimated an enrichment parameter for each annotation individually in the GWAS for **A.** Crohn's disease and **B.** fasting glucose. Shown are the maximum likelihood estimates and 95% confidence intervals. Annotations are ranked according to how much each improves the fit of the model; shown are the 50 annotations that most improve the model (or if there were less than 50 significant annotations, all of the significant annotations). In red are the annotations included in the combined model, and in pink are annotations that are statistically equivalent to those in the combined model.

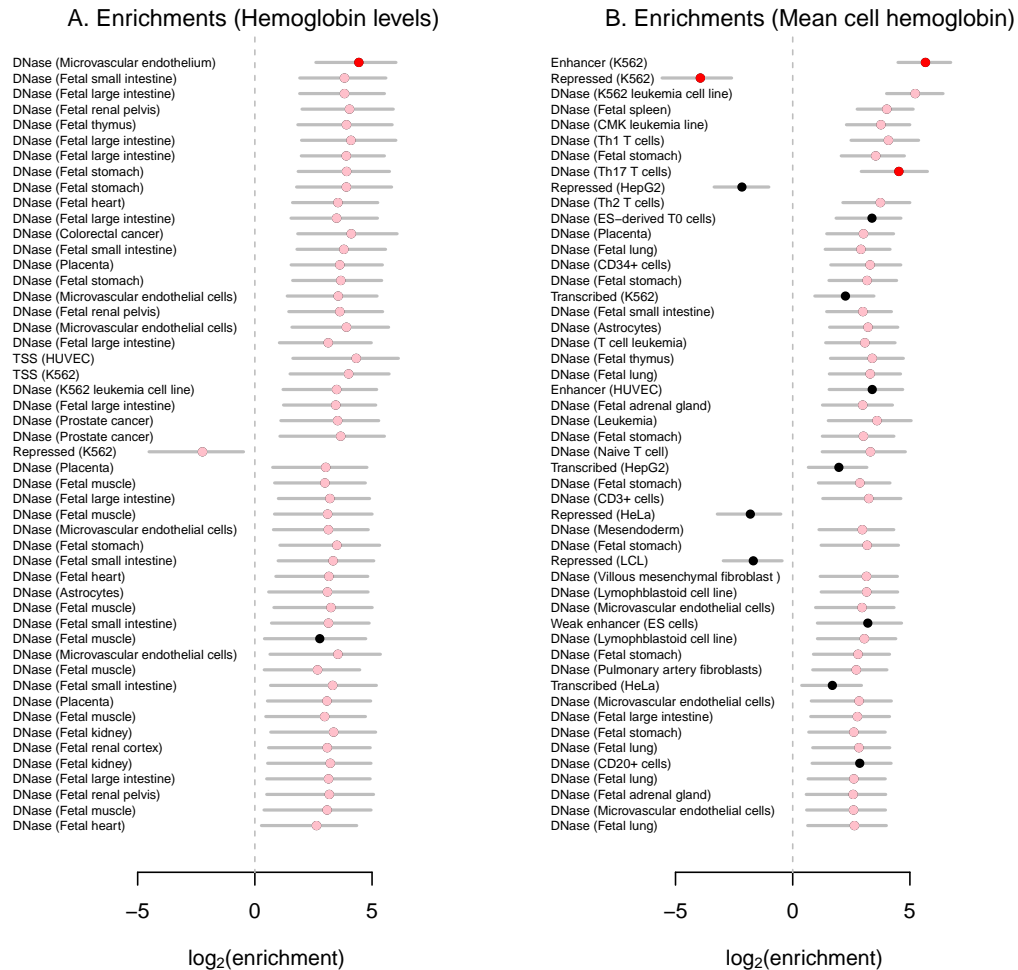


Figure 7. **Annotation effects in the red blood cell data.** We estimated an enrichment parameter for each annotation individually in the GWAS for **A.** hemoglobin levels and **B.** mean cellular hemoglobin. Shown are the maximum likelihood estimates and 95% confidence intervals. Annotations are ranked according to how much each improves the fit of the model; shown are the 50 annotations that most improve the model (or if there were less than 50 significant annotations, all of the significant annotations). In red are the annotations included in the combined model, and in pink are annotations that are statistically equivalent to those in the combined model.

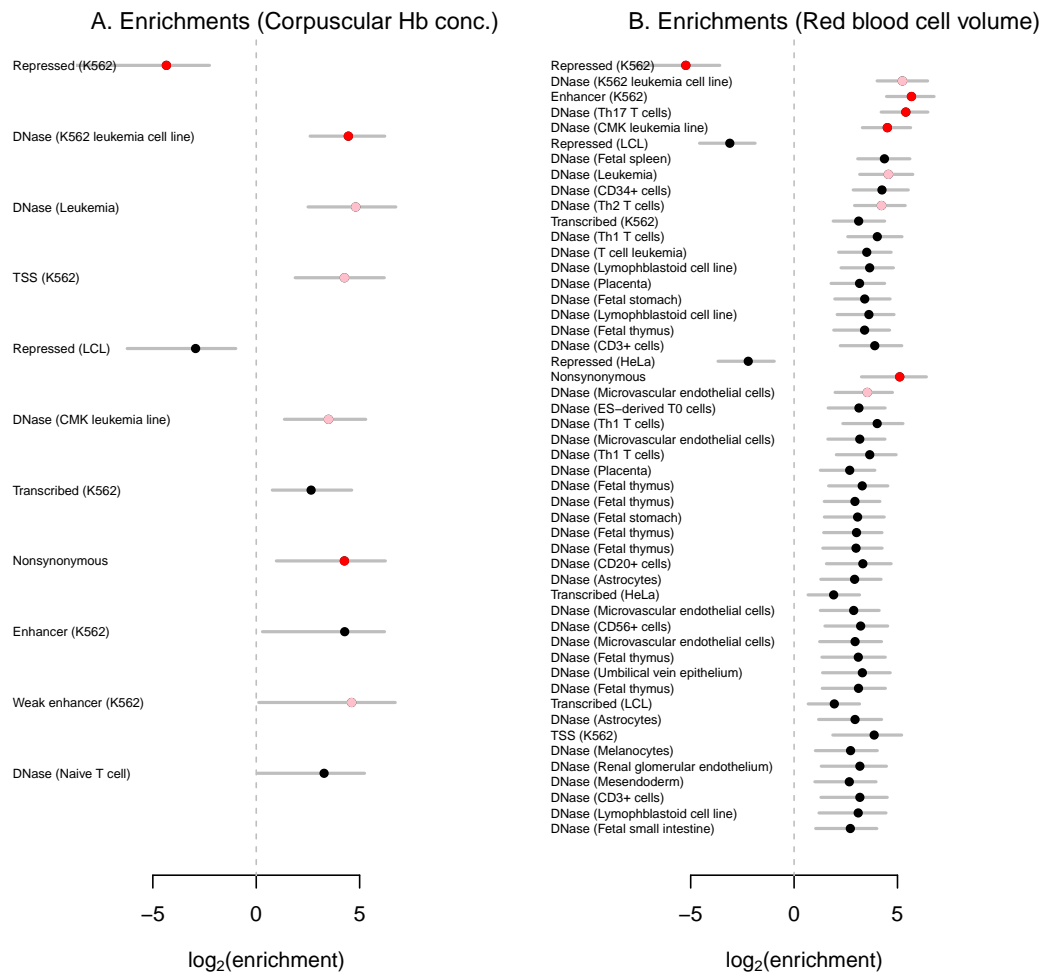


Figure 8. **Annotation effects in the red blood cell data.** We estimated an enrichment parameter for each annotation individually in the GWAS for **A.** mean corpuscular hemoglobin concentration and **B.** mean red cell volume. Shown are the maximum likelihood estimates and 95% confidence intervals. Annotations are ranked according to how much each improves the fit of the model; shown are the 50 annotations that most improve the model (or if there were less than 50 significant annotations, all of the significant annotations). In red are the annotations included in the combined model, and in pink are annotations that are statistically equivalent to those in the combined model.

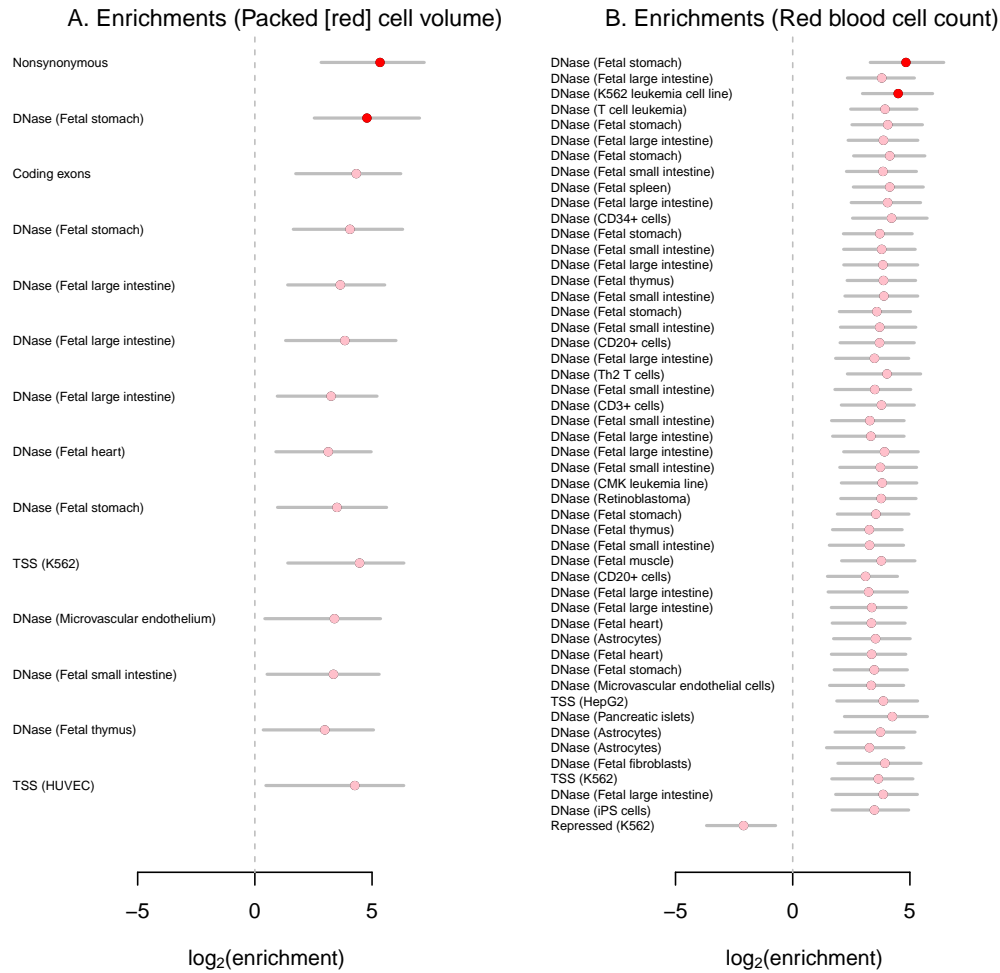


Figure 9. **Annotation effects in the red blood cell data.** We estimated an enrichment parameter for each annotation individually in the GWAS for **A.** packed cell volume and **B.** mean red cell count. Shown are the maximum likelihood estimates and 95% confidence intervals. Annotations are ranked according to how much each improves the fit of the model; shown are the 50 annotations that most improve the model (or if there were less than 50 significant annotations, all of the significant annotations). In red are the annotations included in the combined model, and in pink are annotations that are statistically equivalent to those in the combined model.

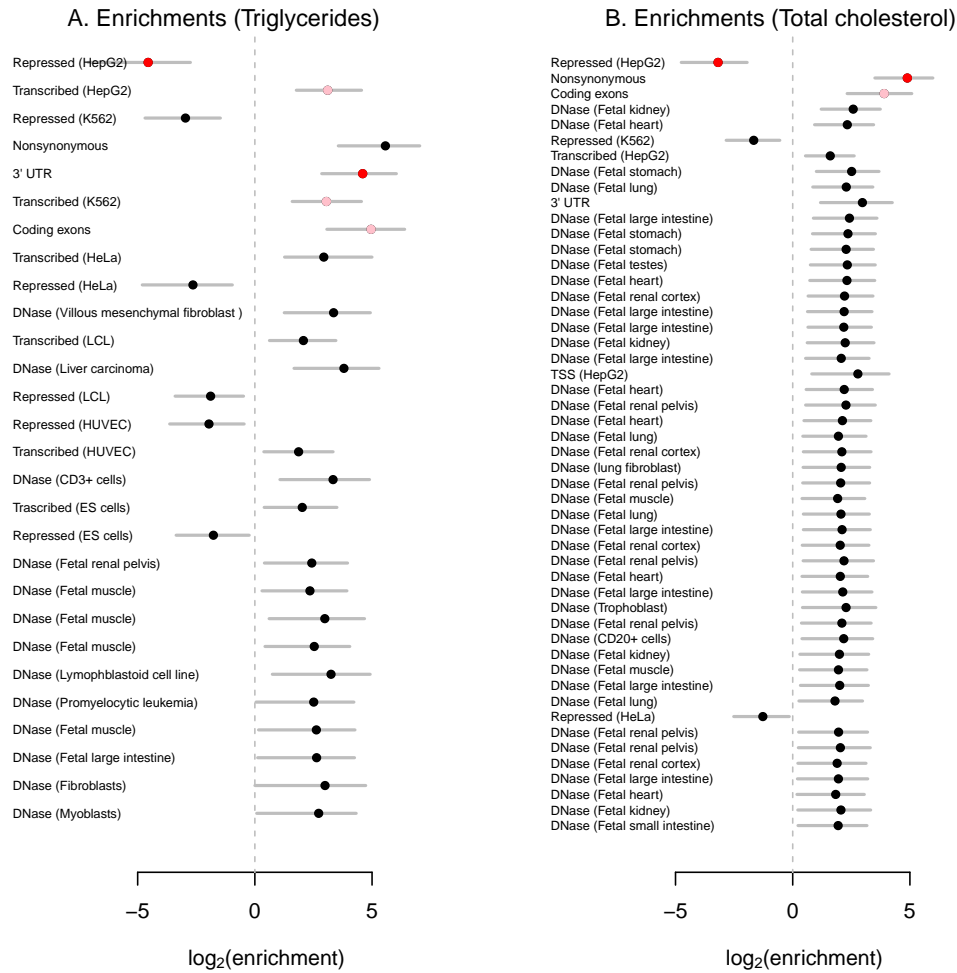


Figure 10. **Annotation effects in the lipids data.** We estimated an enrichment parameter for each annotation individually in the GWAS for **A.** triglyceride levels and **B.** total cholesterol. Shown are the maximum likelihood estimates and 95% confidence intervals. Annotations are ranked according to how much each improves the fit of the model; shown are the 50 annotations that most improve the model (or if there were less than 50 significant annotations, all of the significant annotations). In red are the annotations included in the combined model, and in pink are annotations that are statistically equivalent to those in the combined model.

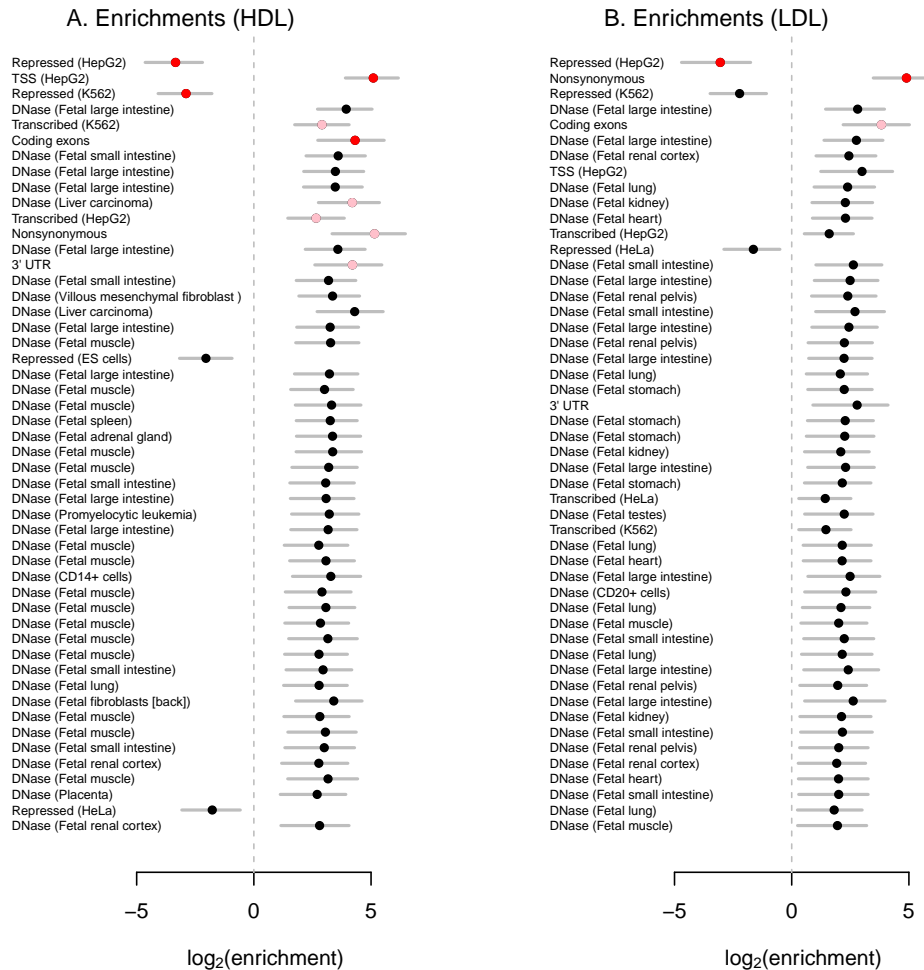


Figure 11. **Annotation effects in the lipids data.** We estimated an enrichment parameter for each annotation individually in the GWAS for **A.** HDL levels and **B.** LDL levels. Shown are the maximum likelihood estimates and 95% confidence intervals. Annotations are ranked according to how much each improves the fit of the model; shown are the 50 annotations that most improve the model (or if there were less than 50 significant annotations, all of the significant annotations). In red are the annotations included in the combined model, and in pink are annotations that are statistically equivalent to those in the combined model.

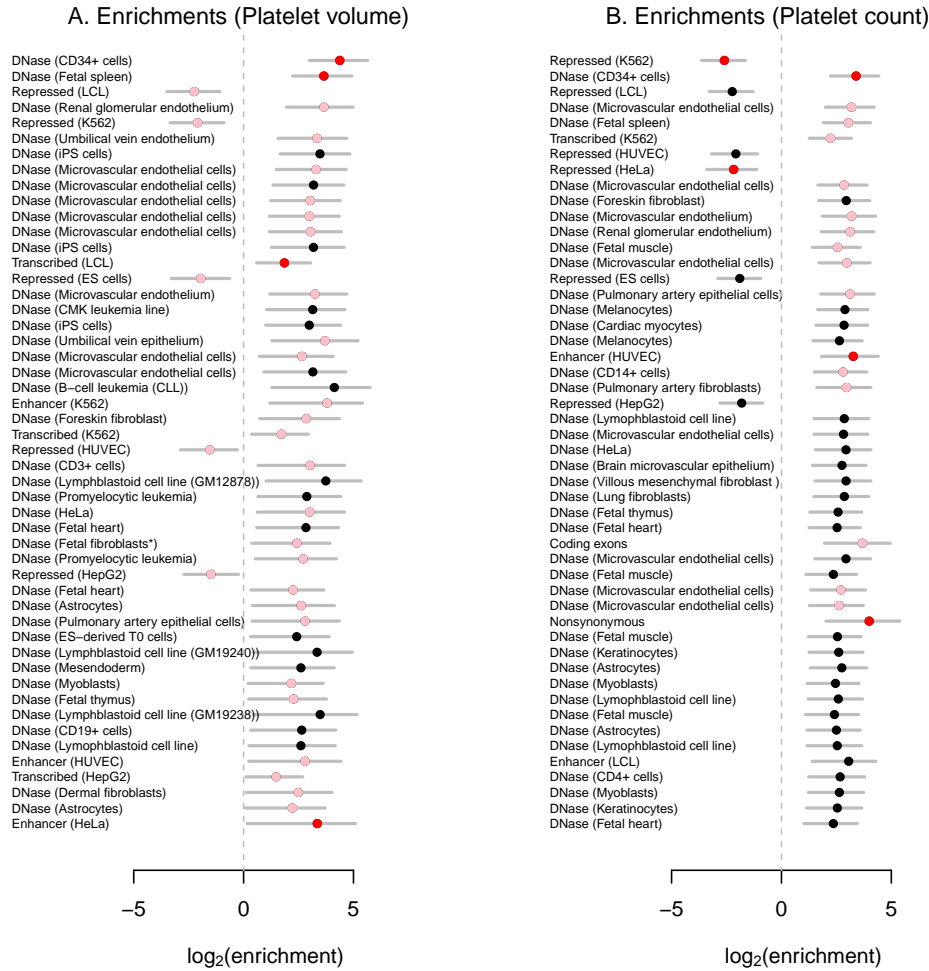


Figure 12. **Annotation effects in the platelet data.** We estimated an enrichment parameter for each annotation individually in the GWAS for **A.** mean platelet volume and **B.** platelet count. Shown are the maximum likelihood estimates and 95% confidence intervals. Annotations are ranked according to how much each improves the fit of the model; shown are the 50 annotations that most improve the model (or if there were less than 50 significant annotations, all of the significant annotations). In red are the annotations included in the combined model, and in pink are annotations that are statistically equivalent to those in the combined model.

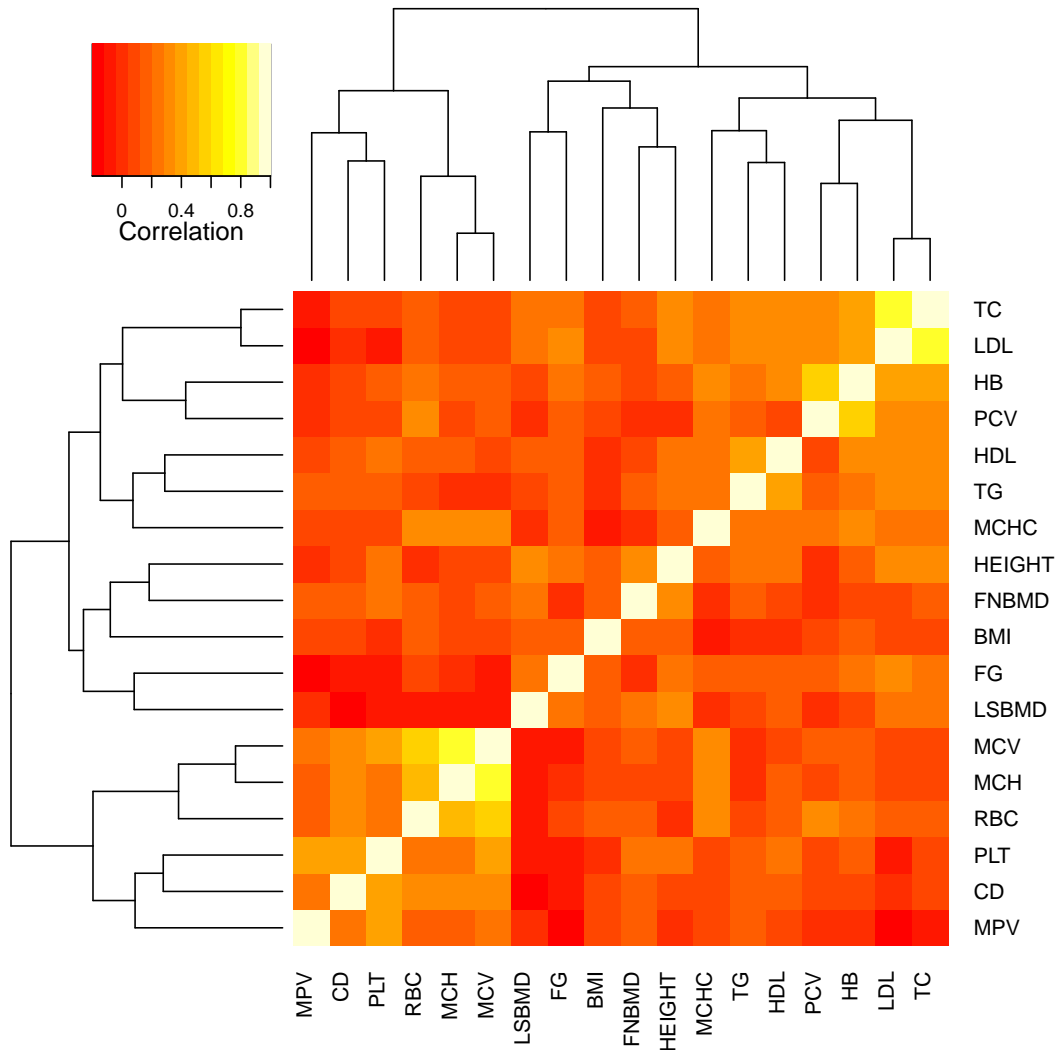


Figure 13. **Correlated patterns of enrichment across traits.** We estimated an enrichment parameter for each of 450 annotations for each of the 18 traits. For each pair of traits, we then estimated the Spearman correlation coefficient between the enrichment parameters. Plotted are these correlation coefficients. Orders of rows and columns were chosen by hierarchical clustering in R [R Core Team, 2013].

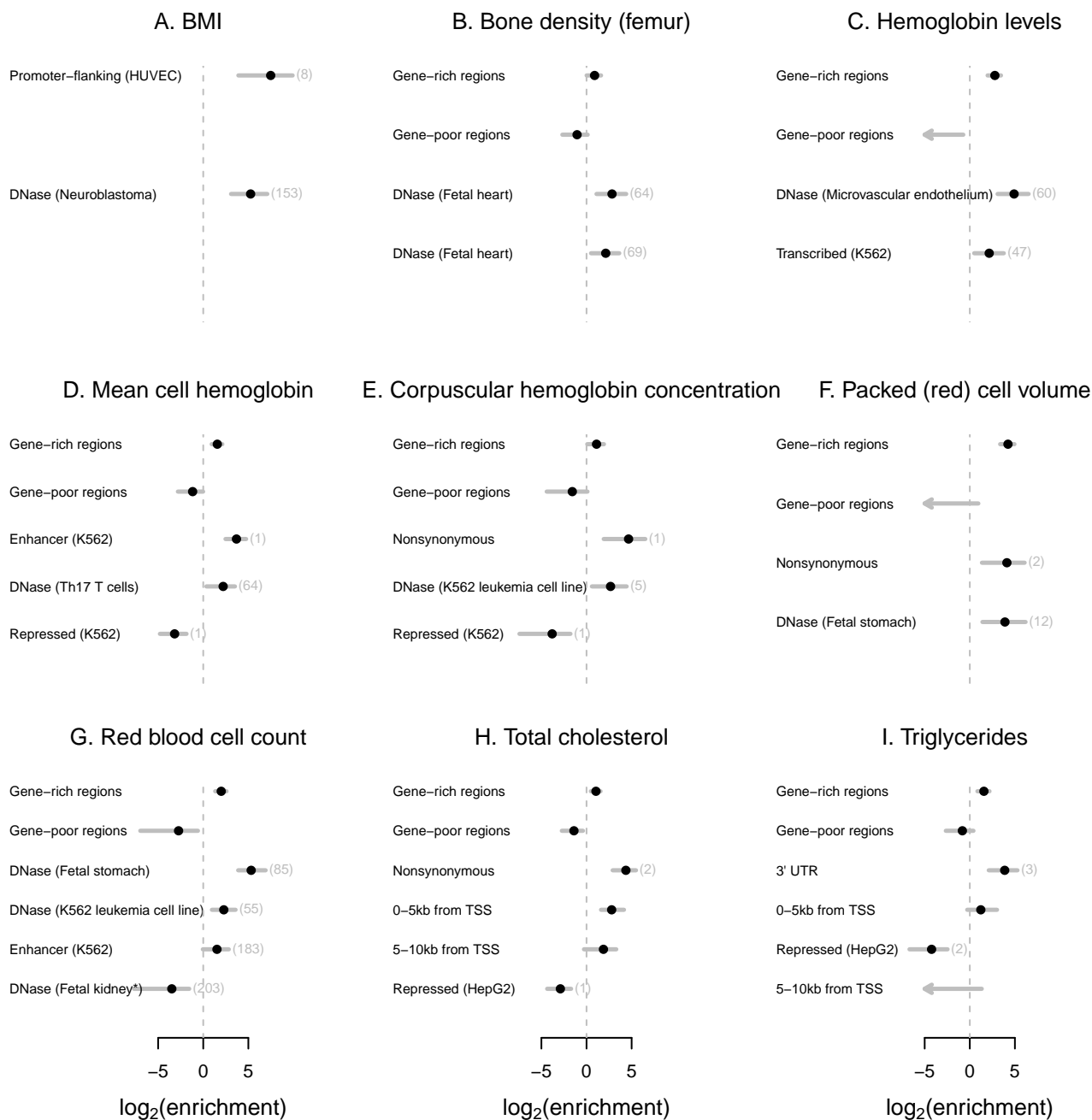


Figure 14. **Combined models for nine traits.** For each trait, we built a combined model of annotations using the algorithm presented in the Methods from the main text. Shown are the maximum likelihood estimates and 95% confidence intervals for all annotations included in each model. Note that though these are the maximum likelihood estimates, model choice was done using a penalized likelihood. In parentheses next to each annotation (except for those relating to distance to transcription start sites), we show the total number of annotations that are statistically equivalent to the included annotation in a conditional analysis. For the other nine traits, see Figure 4 in the main text. *This annotation of DNase-I hypersensitive sites in fetal kidney (renal pelvis) has a positive effect when treated alone; see Supplementary Text for discussion.

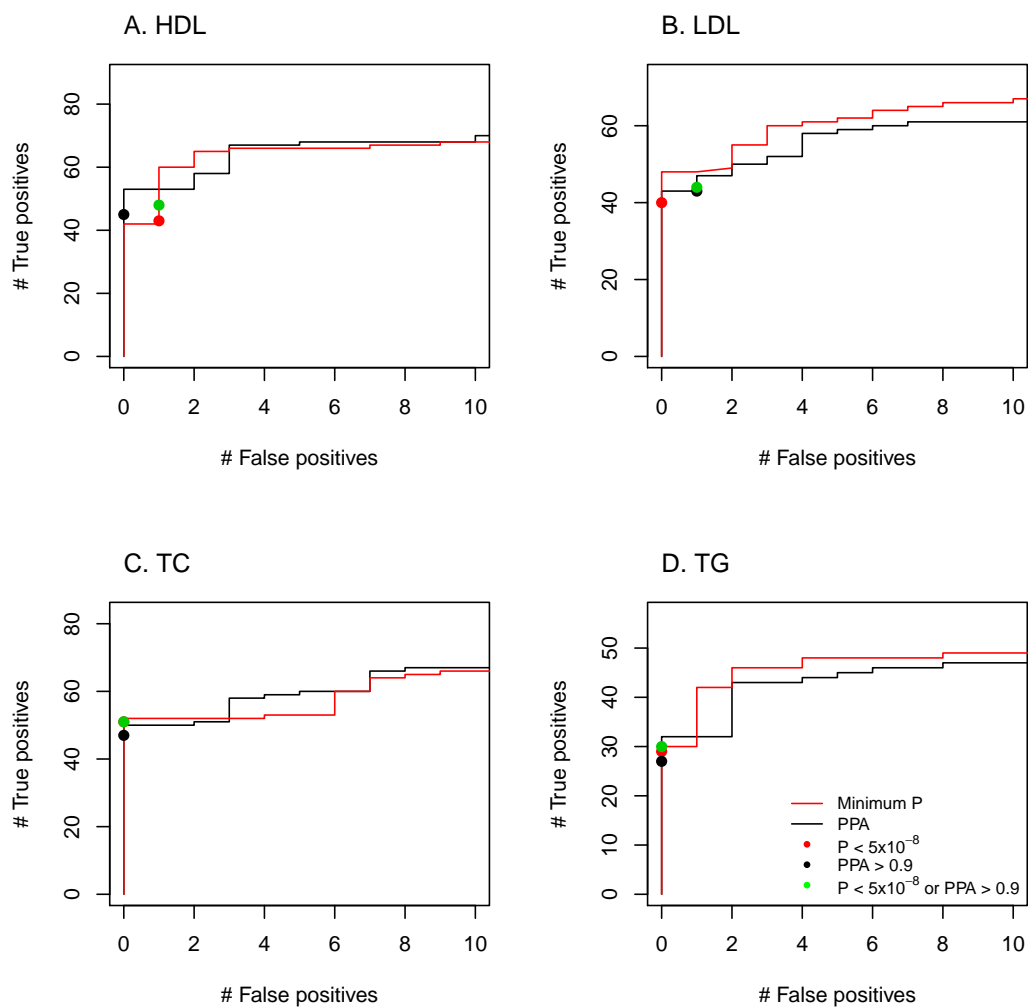


Figure 15. **Calibrating a PPA threshold similar to a P-value threshold.** For each of the four phenotypes in the lipids data, we plot the number of “true positives” and “false positives” obtained by different statistical thresholds; see Supplementary Text for details. Points show the positions of the thresholds used in the paper.

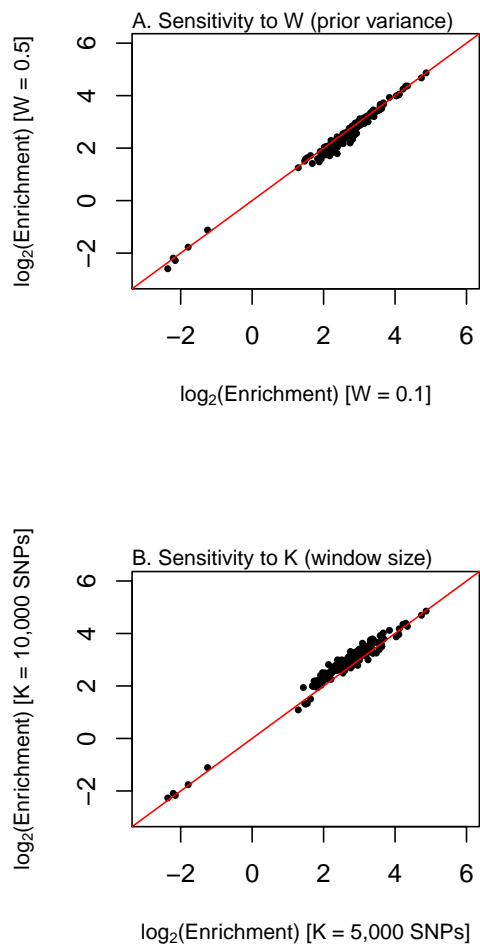


Figure 16. **Robustness of parameter estimates to preset parameters.** **A. Prior variance on effect size.** We estimated an enrichment parameter for each annotation in Crohn’s disease using prior variances of 0.1 or 0.5. Shown are the estimates for all annotations with 95% confidence intervals that did not overlap 0 in at least one of the two runs. In red is the $y = x$ line. **B. Window size.** We estimated an enrichment parameter for each annotation in Crohn’s disease using window sizes of 5,000 and 10,000 SNPs. Shown are the estimates for all annotations with 95% confidence intervals that did not overlap 0 in at least one of the two runs. In red is the $y = x$ line.

Phenotype	λ_{GC} (before imputation)	λ_{GC} (after imputation)
Height	1.04	0.99
BMI	1.04	0.97
BMD (femoral neck)	1.0	0.92
BMD (lumbar spine)	1.0	0.93
Crohn's	1.27	0.71
FG	1.08	0.97
HB	1.07	0.99
MCH	1.13	1.0
MCHC	1.07	0.85
MCV	1.13	1.0
PCV	1.09	0.97
RBC	1.14	1.01
TC	1.0	0.93
TG	1.0	0.92
HDL	1.0	0.94
LDL	1.0	0.93
PLT	1.08	1.01
MPV	1.04	0.96

Table 1: **Genomic control inflation factors before and after imputation.** We show λ_{GC} [Bacanu et al., 2002] before and after imputation for all 18 GWAS included in this study.

Phenotype	Proportion [95% CI]
BMI	0.022 [0.013, 0.032]
FNBMD	0.028 [0.019, 0.040]
LSBMD	0.028 [0.019, 0.041]
Crohn's	0.078 [0.059, 0.10]
FG	0.020 [0.012, 0.03]
HB	0.010 [0.006, 0.015]
HDL	0.034 [0.026, 0.044]
Height	0.131 [0.111, 0.153]
LDL	0.034 [0.026, 0.045]
MCH	0.035 [0.025, 0.047]
MCHC	0.018 [0.011, 0.027]
MCV	0.046 [0.034, 0.059]
MPV	0.025 [0.017, 0.035]
PCV	0.003 [0.002, 0.005]
PLT	0.036 [0.028, 0.047]
RBC	0.023 [0.016, 0.033]
TC	0.052 [0.040, 0.067]
TG	0.023 [0.015, 0.032]

Table 2: **Estimates of the fraction of regions containing an associated SNP for each phenotype.** We show the estimates of $\frac{1}{1+e^{-\kappa}}$, the proportion of regions from the middle third of the distribution of gene density that contain associated SNPs (see Equation 7 in the main text), along with the 95% confidence interval of this parameter.

Annotation	Description	$\log_2(\text{Effect})$ [95% CI]	Penalized effect	Marginal effect [95% CI]
BE2_C-DS14625	DNase-I in BE(2)-C neuroblastoma cell line	5.25 [3.09, 7.10]	5.15	5.60 [3.51, 7.47]
HUVEC PF	Genome segmentation in HUVEC cells: promoter-flanking	7.47 [3.90,9.91]	7.18	8.51 [5.41, 10.62]

Table 3: **Combined model learned for BMI.** Shown are the exact annotation names and parameters learned for BMI, along with the penalized effect sizes and the effect of each annotation in a single-annotation model.

Annotation	Description	$\log_2(\text{Effect})$ [95% CI]	Penalized effect	Marginal effect [95% CI]
High gene density	Regional annotation: top 1/3 of gene density	0.89 [0.01, 1.62]	0.88	NA
Low gene density	Regional annotation: bottom 1/3 of gene density	-1.05 [-2.68, 0.12]	-0.95	NA
fHeart-DS12810	DNase-I in fetal heart	2.83 [1.11, 4.40]	2.45	4.83 [3.08, 6.43]
fHeart-DS16621	DNase-I in fetal heart	2.12 [0.50, 3.64]	2.21	4.47 [2.76, 6.03]

Table 4: **Combined model learned for bone mineral density (femur).** Shown are the exact annotation names and parameters learned for FNBMD, along with the penalized effect sizes and the effect of each annotation in a single-annotation model.

Annotation	Description	$\log_2(\text{Effect})$ [95% CI]	Penalized effect	Marginal effect [95% CI]
High gene density	Regional annotation: top 1/3 of gene density	0.52 [-0.40, 1.27]	0.53	NA
Low gene density	Regional annotation: bottom 1/3 of gene density	-1.49 [-3.65, -0.13]	-1.33	NA
HSMMD-DS15542	DNase-I in skeletal muscle myoblasts	4.23 [2.24, 5.97]	3.75	3.90 [1.98, 5.58]

Table 5: **Combined model learned for bone mineral density (spine).** Shown are the exact annotation names and parameters learned for LSBMD, along with the penalized effect sizes and the effect of each annotation in a single-annotation model.

Annotation	Description	$\log_2(\text{Effect})$ Effect [95% CI]	Penalized effect	Marginal effect [95%
High gene density	Regional annotation: top 1/3 of gene density	1.18 [0.61, 1.72]	1.18	NA
Low gene density	Regional annotation: bottom 1/3 of gene density	-2.18 [-4.10, -0.92]	-2.03	NA
fSkin_fibro_upper_back-DS19696	DNase-I in fetal skin fibroblasts from the upper back	5.21 [4.08, 6.20]	4.78	3.84 [2.63, 4.89]
gm12878.combined.R	Genome segmentation of GM12878: repressed	-1.83 [-3.06, -0.78]	-1.79	-2.35 [-4.50, -1.05]
fSkin_fibro_abdomen-DS19561	DNase-I in fetal skin fibroblasts from abdomen	-2.34 [-3.85, -1.18]	-1.86	2.77 [1.27, 3.94]
huvec.combined.T	Genome segmentation of HUVEC: transcribed	1.20 [0.25, 2.15]	1.17	1.63 [0.61, 2.65]
Distance to TSS [0-5 kb]	From 0-5 kb from a TSS	1.18 [0.17, 2.15]	1.17	NA
Distance to TSS [5-10 kb]	From 5-10 kb from a TSS	0.45 [-1.38, 1.75]	0.40	NA

Table 6: **Combined model learned for Crohn’s disease.** Shown are the exact annotation names and parameters learned for Crohn’s disease, along with the penalized effect sizes and the effect of each annotation in a single-annotation model.

Annotation	Description	$\log_2(\text{Effect})$ [95% CI]	Penalized effect	Marginal effect [95% CI]
fStomach-DS17878	DNase-I in fetal stomach	3.66 [1.66, 5.31]	3.62	3.82 [1.66, 5.50]
Nonsynonymous	nonsynonymous SNPs	4.28 [1.53, 6.10]	4.13	4.95 [1.40, 6.95]
Distance to TSS [0-5 kb]	From 0-5 kb from a TSS	1.83 [0.22, 3.40]	1.75	NA
Distance to TSS [5-10 kb]	From 5-10 kb from a TSS	2.68 [0.76, 4.28]	2.54	NA

Table 7: **Combined model learned for fasting glucose.** Shown are the exact annotation names and parameters learned for FG, along with the penalized effect sizes and the effect of each annotation in a single-annotation model.

Annotation	Description	$\log_2(\text{Effect})$ 95% CI]	Penalized effect	Marginal effect [95% CI]
High gene density	Regional annotation: top 1/3 of gene density	2.78 [1.98, 3.46]	2.80	NA
Low gene density	Regional annotation: bottom 1/3 of gene density	-40.6 [- inf, -0.72]	-5.44	NA
HMVEC_dAd-DS12957	DNase-I in microvascular endothelium	4.91 [3.09, 6.52]	4.86	4.43 [2.60, 6.02]
k562.combined.T	Genome segmentation of K562: transcribed	2.15 [0.49, 3.77]	2.12	1.82 [0.01, 3.55]

Table 8: **Combined model learned for hemoglobin levels.** Shown are the exact annotation names and parameters learned for hemoglobin levels, along with the penalized effect sizes and the effect of each annotation in a single-annotation model.

Annotation	Description	$\log_2(\text{Effect})$ [95% CI]	Penalized effect	Marginal effect [95% CI]
High gene density	Regional annotation: top 1/3 of gene density	1.69 [1.13, 2.19]	1.56	NA
Low gene density	Regional annotation: bottom 1/3 of gene density	-1.17 [-0.13, 0.69]	-0.20	NA
hepg2.combined.R	Genome segmentation of HepG2: repressed	-1.83 [-3.12, -0.68]	-1.79	-3.35 [-4.63, -2.19]
hepg2.combined.TSS	Genome segmentation of HepG2: TSS	3.10 [1.79, 4.20]	2.84	5.09 [3.91, 6.16]
ens_coding_exons	Ensembl: coding exons	3.16 [1.51, 4.40]	2.73	4.31 [2.73, 5.55]
k562.combined.R	Genome segmentation of K562: repressed	-1.43 [-2.65, -0.30]	-1.43	-2.90 [-4.08, -1.79]

Table 9: **Combined model learned for HDL levels.** Shown are the exact annotation names and parameters learned for HDL, along with the penalized effect sizes and the effect of each annotation in a single-annotation model.

Annotation	Description	$\log_2(\text{Effect})$ [95% CI]	Penalized effect	Marginal effect [95% CI]
High gene density	Regional annotation: top 1/3 of gene density	1.50 [1.13, 1.86]	1.49	NA
Low gene density	Regional annotation: bottom 1/3 of gene density	-0.95 [-1.62, -0.36]	-0.94	NA
helas3.combined.R	Genome segmentation of HeLa: repressed	-1.50 [-2.39, -0.71]	-1.50	-2.74 [-3.78, -1.85]
fMuscle_lower_limb-DS18174	DNase-I in fetal muscle from lower limb	2.27 [1.50, 3.02]	2.24	3.61 [2.81, 4.40]
Nonsynonymous	Nonsynonymous SNPs	3.74 [2.55, 4.65]	3.58	4.27 [2.77, 5.32]
fLung-DS15573	DNase-I in fetal lung	2.09 [1.30, 2.80]	2.05	3.77 [2.97, 4.50]
huvec.combined.T	Genome segmentation of HUVEC: transcribed	1.27 [0.52, 1.96]	1.24	1.63 [0.89, 2.34]
ens_utr3_exons	Ensembl: 3' UTRs	1.57 [0.00, 2.64]	1.54	2.93 [1.34, 3.98]

Table 10: **Combined model learned for height.** Shown are the exact annotation names and parameters learned for height, along with the penalized effect sizes and the effect of each annotation in a single-annotation model.

Annotation	Description	$\log_2(\text{Effect})$ [95% CI]	Penalized effect	Marginal effect [95% CI]
High gene density	Regional annotation: top 1/3 of gene density	1.77 [1.21, 2.27]	1.72	NA
Low gene density	Regional annotation: bottom 1/3 of gene density	-0.72 [-1.98, 0.25]	-0.71	NA
hepg2.combined.R	Genome segmentation of HepG2: repressed	-2.78 [-4.36, -1.51]	-2.70	-3.04 [-4.70, -1.76]
Nonsynonymous	Nonsynonymous SNPs	4.24 [2.74, 5.40]	3.97	4.89 [3.48, 6.02]
Distance to TSS [0-5 kb]	From 0-5 kb from a TSS	3.13 [1.96, 4.56]	2.84	NA
Distance to TSS [5-10 kb]	From 5-10 kb from a TSS	1.63 [-0.65, 3.12]	1.17	NA

Table 11: **Combined model learned for LDL levels.** Shown are the exact annotation names and parameters learned for LDL, along with the penalized effect sizes and the effect of each annotation in a single-annotation model.

Annotation	Description	$\log_2(\text{Effect})$ [95% CI]	Penalized effect	Marginal effect [95% CI]
High gene density	Regional annotation: top 1/3 of gene density	1.56 [0.94, 2.11]	1.51	NA
Low gene density	Regional annotation: bottom 1/3 of gene density	-1.17 [-2.80, -0.01]	-1.10	NA
k562.combined.E	Genome segmentation of K562: enhancers	3.68 [2.47, 4.75]	3.53	5.67 [4.49, 6.74]
k562.combined.R	Genome segmentation of K562: repressed	-3.17 [-4.80, -1.86]	-2.97	-3.94 [-5.57, -2.61]
hTH17-DS11039	DNase-I in Th17 T cells	2.21 [0.35, 3.51]	2.06	4.53 [2.93, 5.74]

Table 12: **Combined model learned for mean cell hemoglobin.** Shown are the exact annotation names and parameters learned for MCH, along with the penalized effect sizes and the effect of each annotation in a single-annotation model.

Annotation	Description	$\log_2(\text{Effect})$ [95% CI]	Penalized effect	Marginal effect [95% CI]
High gene density	Regional annotation: top 1/3 of gene density	1.11 [0.09, 1.93]	1.17	NA
Low gene density	Regional annotation: bottom 1/3 of gene density	-1.57 [-4.41, 0.10]	-1.36	NA
k562.combined.R	Genome segmentation of K562: repressed	-3.81 [-7.43, -1.79]	-3.42	-4.34 [-8.94, -2.27]
K562-DS9767	DNase-I in K562 cells	2.67 [0.61, 4.44]	2.47	4.46 [2.60, 6.22]
Nonsynonymous	Nonsynonymous SNPs	4.66 [1.90, 6.52]	4.03	4.27 [0.97, 6.25]

Table 13: **Combined model learned for mean corpuscular hemoglobin concentration.** Shown are the exact annotation names and parameters learned for MCHC, along with the penalized effect sizes and the effect of each annotation in a single-annotation model.

Annotation	Description	$\log_2(\text{Effect})$ [95% CI]	Penalized effect	Marginal effect [95% CI]
High gene density	Regional annotation: top 1/3 of gene density	1.36 [0.76, 1.86]	1.31	NA
Low gene density	Regional annotation: bottom 1/3 of gene density	-1.51 [-3.06, -0.39]	-1.46	NA
k562.combined.R	Genome segmentation of K562: repressed	-3.91 [-6.25, -2.38]	-3.69	-5.24 [-7.76, -3.59]
k562.combined.E	Genome segmentation of K562: enhancer	3.10 [1.86, 4.15]	2.96	5.67 [4.47, 6.77]
hTH17-DS11039	DNase-I in Th17 T cells	2.31 [0.81, 3.48]	2.25	5.40 [4.21, 6.46]
Nonsynonymous	Nonsynonymous SNPs	4.54 [2.34, 5.92]	4.13	5.11 [3.26, 6.39]
CMK-DS12393	DNase-I in CMK leukemia line	1.28 [0.04, 2.35]	1.34	4.52 [3.30, 5.64]
Distance to TSS [0-5 kb]	From 0-5 kb from a TSS	0.38 [-1.59, 0.65]	-0.33	NA
Distance to TSS [5-10 kb]	From 5-10 kb from a TSS	0.89 [-0.40, 1.83]	0.84	NA

Table 14: **Combined model learned for mean red cell volume.** Shown are the exact annotation names and parameters learned for MCV, along with the penalized effect sizes and the effect of each annotation in a single-annotation model.

Annotation	Description	$\log_2(\text{Effect})$ [95% CI]	Penalized effect	Marginal effect [95% CI]
High gene density	Regional annotation: top 1/3 of gene density	1.95 [1.30, 2.52]	1.88	NA
Low gene density	Regional annotation: bottom 1/3 of gene density	-2.06 [-4.73, -0.40]	-1.63	NA
CD34-DS12274	DNase-I in CD34+ cells	3.02 [1.69, 4.26]	2.76	4.37 [2.99, 5.64]
gm12878.combined.T	Genome segmentation of GM12878: transcribed	2.35 [1.07, 3.53]	1.83	1.86 [0.59, 3.04]
helas3.combined.E	Genome segmentation of HeLa: enhancer	2.80 [0.75, 4.23]	2.27	3.35 [0.16, 5.09]
fSpleen-DS17448	DNase-I in fetal spleen	1.93 [0.59, 3.15]	1.88	3.65 [2.22, 4.92]

Table 15: **Combined model learned for mean platelet volume.** Shown are the exact annotation names and parameters learned for MPV, along with the penalized effect sizes and the effect of each annotation in a single-annotation model.

Annotation	Description	$\log_2(\text{Effect})$ [95% CI]	Penalized effect	Marginal effect [95% CI]
High gene density	Regional annotation: top 1/3 of gene density	4.24 [3.36, 4.95]	3.72	NA
Low gene density	Regional annotation: bottom 1/3 of gene density	-40.60 [-inf, 0.94]	-1.92	NA
Nonsynonymous	Nonsynonymous SNPs	4.11 [1.34, 6.07]	3.61	5.34 [2.83, 7.23]
fStomach-DS17172	DNase-I in fetal stomach	3.90 [1.40, 6.17]	3.48	4.78 [2.54, 7.03]

Table 16: **Combined model learned for packed red cell volume.** Shown are the exact annotation names and parameters learned for PCV, along with the penalized effect sizes and the effect of each annotation in a single-annotation model.

Annotation	Description	$\log_2(\text{Effect})$ [95% CI]	Penalized effect	Marginal effect [95% CI]
High gene density	Regional annotation: top 1/3 of gene density	1.67 [2.81, 2.64]	2.14	NA
Low gene density	Regional annotation: bottom 1/3 of gene density	-1.63 [-3.40, -0.38]	-1.51	NA
k562.combined.R	Genome segmentation in K562: repressed	-1.60 [-2.63, -0.66]	-1.60	-2.60 [-3.65, -1.64]
CD34-DS12274	DNase-I in CD34+ cells	1.82 [0.59, 2.86]	1.80	3.39 [2.24, 4.43]
Nonsynonymous	Nonsynonymous SNPs	3.38 [1.31, 4.79]	3.00	3.98 [2.02, 5.38]
huvec.combined.E	Genome segmentation in HUVEC: enhancers	1.67 [0.16, 2.84]	1.59	3.27 [1.82, 4.41]
helas3.combined.R	Genome segmentation in HeLa: repressed	-1.17 [-2.37, -0.13]	-1.14	-2.18 [-3.40, -1.11]

Table 17: **Combined model learned for platelet count.** Shown are the exact annotation names and parameters learned for PLT, along with the penalized effect sizes and the effect of each annotation in a single-annotation model.

Annotation	Description	$\log_2(\text{Effect})$ [95% CI]	Penalized effect	Marginal effect [95% CI]
High gene density	Regional annotation: top 1/3 of gene density	1.99 [1.33, 2.58]	1.96	NA
Low gene density	Regional annotation: bottom 1/3 of gene density	-2.74 [-6.97, -0.59]	-2.18	NA
fStomach-DS17878	DNase-I in fetal stomach	5.31 [3.87, 6.91]	4.83	4.83 [3.30, 6.45]
k562.combined.E	Genome segmentation of K562: enhancer	1.53 [-0.04, 2.83]	1.56	4.28 [1.41, 5.90]
fKidney_renal_pelvis_R-DS18663	DNase-I in fetal renal pelvis	-3.49 [-7.68, -1.56]	-2.80	2.48 [0.04, 4.17]
K562-DS9767	DNase-I in K562 leukemia line	2.28 [0.97, 3.58]	2.25	4.50 [2.97, 5.97]

Table 18: **Combined model learned for red blood cell count.** Shown are the exact annotation names and parameters learned for RBC, along with the penalized effect sizes and the effect of each annotation in a single-annotation model.

Annotation	Description	$\log_2(\text{Effect})$ [95% CI]	Penalized effect	Marginal effect [95% CI]
High gene density	Regional annotation: top 1/3 of gene density	1.05 [0.48, 1.56]	1.04	NA
Low gene density	Regional annotation: bottom 1/3 of gene density	-1.40 [-2.74, -0.39]	-1.34	NA
hepg2.combined.R	Genome segmentation of HepG2: repressed	-2.90 [-4.36, -1.72]	-2.84	-3.19 [-4.76, -1.95]
Nonsynonymous	Nonsynonymous SNPs	4.36 [2.90, 5.48]	4.18	4.89 [3.51, 5.99]
Distance to TSS [0-5 kb]	From 0-5 kb from a TSS	2.76 [1.62, 4.15]	2.58	NA
Distance to TSS [5-10 kb]	From 5-10 kb from a TSS	1.88 [-0.27, 3.29]	1.56	NA

Table 19: **Combined model learned for total cholesterol.** Shown are the exact annotation names and parameters learned for total cholesterol, along with the penalized effect sizes and the effect of each annotation in a single-annotation model.

Annotation	Description	$\log_2(\text{Effect})$ [95% CI]	Penalized effect	Marginal effect [95% CI]
High gene density	Regional annotation: top 1/3 of gene density	1.56 [0.85, 2.18]	1.49	NA
Low gene density	Regional annotation: bottom 1/3 of gene density	-0.82 [-2.65, 0.40]	-0.78	NA
hepg2.combined.R	Genome segmentation of HepG2: repressed	-4.24 [-6.68, -2.47]	-3.75	-4.56 [-7.11, -2.76]
ens_utr3_exons	Ensembl: 3' UTRs	3.87 [2.11, 5.28]	3.46	4.60 [2.86, 6.03]

Table 20: **Combined model learned for triglyceride levels.** Shown are the exact annotation names and parameters learned for triglycerides, along with the penalized effect sizes and the effect of each annotation in a single-annotation model.

Phenotype	PPA		P-value		combined	
	True positives	False positives	True positives	False positives	True positives	False positives
HDL	45	0	43	1	48	1
LDL	43	1	40	0	44	1
TC	47	0	51	0	51	0
TG	27	0	29	0	30	0

Table 21: **Comparison of loci identified in the lipids data with different methods.** We ranked genomic regions in GWAS of four lipid traits according to their minimum P-value or posterior probability of association from Teslovich et al. [2010]. We then evaluated false positives and false negatives by comparison to a larger GWAS [Global Lipids Genetics Consortium et al., 2013]. See Supplementary Text for details.

trait	region (hg19)	Regional PPA	lead SNP (P-value)	Nearest gene	Successful replication (SNP, r^2 with lead)
BMI	chr13:27,75,5426-29,745,954	0.94	rs9512699 (6×10^{-8})	MTIF3	[Speliotes et al., 2010] (rs4771122, 0.73)
BMD (femur)	chr1:170,892-281-173,086,517	0.93	rs6701929 (2×10^{-7})	DNM3	[Estrada et al., 2012] (rs479336, 0.93)
HDL	chr1:25,427,217-29,426,896	0.96	rs6659176 (1.5×10^{-6})	NR0B2	[Global Lipids Genetics Consortium et al., 2013] (rs12748152, 0.85)
HDL	chr1:93,534,311-95,828,501	0.93	rs2297707 (1×10^{-6})	TMED5	[Global Lipids Genetics Consortium et al., 2013] (rs12133576, 0.79)
HDL	chr1:108,743,042-111,481,349	0.97	rs12740374 (6×10^{-8})	CELSR2	[Global Lipids Genetics Consortium et al., 2013] (rs12740374)
HDL	chr2:85,349,339-88,736,950	0.98	rs1044973 (1.5×10^{-4})	TGOLN2	No (sample size not increased in Global Lipids Genetics Consortium et al. [2013])
HDL	chr10:45,535,916-50,321,467	0.93	rs10900223 (1.4×10^{-7})	MARCH8	[Global Lipids Genetics Consortium et al., 2013] (rs970548, 0.99)
MCV	chr3:139,060,509-141,377,851	0.98	rs13059128 (3.8×10^{-7})	ZBTB38	[van der Harst et al., 2012] (rs6776003, 0.48)
MCV	chr9:134,164,493-136,620,584	0.90	rs8176662 (7.5×10^{-4})	ABO	NA
MCV	chr20:24,615,239-30,836,608	0.98	rs6088962 (7.5×10^{-4})	BCL2L1	NA
TG	chr16:31,050,033-49,644,030	0.95	rs1549293 (2.7×10^{-4})	KAT8	[Global Lipids Genetics Consortium et al., 2013] (rs749671, 0.80)
LDL	chr1:91,146,258-93,672,688	0.97	rs7542747 (2×10^{-4})	RPAP2	[Global Lipids Genetics Consortium et al., 2013] (rs4970712, 0.75)
LDL	chr1:146,751,272-152,014,465	0.98	rs2677733 (7×10^{-8})	ANXA9	[Global Lipids Genetics Consortium et al., 2013] (rs267733)
LDL	chr2:116,901,934-119,001,411	0.98	rs1052639 (6.6×10^{-8})	DDX18	[Global Lipids Genetics Consortium et al., 2013] (rs10490626, 0.53)
LDL	chr13:31,693,235-34,119,073	0.93	rs4942505 (9.8×10^{-8})	BRCA2	[Global Lipids Genetics Consortium et al., 2013] (rs4942505)
LDL	chr17:7,456,344-9,908,665	0.92	rs4791641 (2.6×10^{-4})	PFAS	No ($P = 1.3 \times 10^{-7}$ in [Global Lipids Genetics Consortium et al., 2013])
MCHC	chr7:76,062,644-78,334,941	0.93	rs58176556 (5.4×10^{-8})	PHTF2	NA
Height	chr2:240,701,166-243,060,642	0.98	rs13006939 (3.9×10^{-7})	SEPT2	[Lango-Allen et al., 2010] (rs12694997, 0.99)
Height	chr3:11,167,568-13,294,698	0.98	rs2276749 (3.0×10^{-6})	VGLL2	NA
Height	chr3:13,294,698-15,353,840	0.93	rs2597513 (1.1×10^{-4})	HDAC11	[Lango-Allen et al., 2010] (rs2597513)
Height	chr3:55,068,506-57,000,141	0.94	rs7637449 (1.3×10^{-6})	CCDC66	[Lango-Allen et al., 2010] (rs9835332, 0.87)
Height	chr4:72,048-2,570,837	0.98	rs3958122 (6.0×10^{-8})	SLBP	[Lango-Allen et al., 2010] (rs2247341, 0.99)
Height	chr5:71,376,237-73,712,303	0.98	rs34651 (2.5×10^{-7})	TNPO1	NA
Height	chr6:108,017,102-110,694,347	0.95	rs1476387 (2.2×10^{-6})	SMPD2	[Lango-Allen et al., 2010] (rs1046943, 0.93)
Height	chr7:22,074,248-23,988,552	0.99	rs12534093 (5.6×10^{-8})	IGFBP3	[Lango-Allen et al., 2010] (rs12534093)
Height	chr7:46,327,426-48,083,339	0.97	rs12538905 (2.6×10^{-7})	IGFBP3	NA
Height	chr9:87,279,007-89,667,667	0.90	rs405761 (1.3×10^{-4})	ZCCHC6	[Lango-Allen et al., 2010] (rs8181166, 0.82)
Height	chr11:12,559,691-14,685,886	1.0	rs7926971 (7.3×10^{-8})	TEAD1	[Lango-Allen et al., 2010] (rs7926971)
Height	chr11:14,685,886-17,491,336	0.93	rs757081 (2.2×10^{-6})	NUCB2	[Lango-Allen et al., 2010] (rs1330, 0.60)
Height	chr15:62,349,517-64,370,301	0.97	rs7178424 (2.2×10^{-4})	C2CD4A	[Lango-Allen et al., 2010] (rs178424)
Height	chr17:19,924,256-26,838,292	0.96	rs9895199 (3.6×10^{-4})	KCNJ12	[Lango-Allen et al., 2010] (rs4640244, 0.79)
Height	chr17:45,331,502-47,944,460	0.99	rs9904645 (2.2×10^{-4})	ATP5G1	NA
Height	chr2:22,32,075,899-33,846,972	0.97	rs1012366 (6.9×10^{-8})	SYN3	[Lango-Allen et al., 2010] (rs4821083 not in 1000 Genomes)
Crohn's	chr2:42,522,756-44,575,426	1.0	rs17031095 (2.6×10^{-4})	THADA	[Jostins et al., 2012] (rs10495903, 0.95)
Crohn's	chr10:59,615,595-61,881,674	1.0	rs1832556 (2.0×10^{-4})	IPMK	[Jostins et al., 2012] (rs2790216, 0.94)
Crohn's	chr11:61,269,649-64,734,682	0.98	rs174568 (2.8×10^{-4})	FADS2	[Jostins et al., 2012] (rs4246215, 0.86)
Crohn's	chr13:99,900,420-102,096,823	0.94	rs3742130 (2.3×10^{-6})	GPR18	[Jostins et al., 2012] (rs9557195, 0.91)
Crohn's	chr15:67,140,517-70,199,927	0.93	rs11639295 (6.4×10^{-7})	SMAD3	[Jostins et al., 2012] (rs17293632, 0.10)
Crohn's	chr17:17,986,955-26,038,545	0.92	rs2945406 (4.1×10^{-4})	KSR1	[Jostins et al., 2012] (rs2945412, 0.13)
PLT	chr1:44,022,121-47,087,366	0.99	rs4468203 (3.2×10^{-4})	GPBP1L1	NA
PLT	chr9:90,221,450-92,241,847	0.90	rs9410382 (1.9×10^{-6})	S1PR3	NA
PLT	chr11:32,343,164-34,501,064	0.93	rs7481878 (7.2×10^{-6})	QSER1	NA
MCH	chr4:86,147,717-88,340,969	0.98	rs6819155 (2.3×10^{-7})	APP1	NA
MCH	chr14:102,971,016-107,289,436	0.93	rs17616316 (1.5×10^{-7})	EIF5	[van der Harst et al., 2012] (rs17616316)
HB	chr15:75,349,145-78,654,148	0.90	rs1874953 (4.2×10^{-4})	NRG4	[van der Harst et al., 2012] (rs11072566, 0.93)
BMD (spine)	chr17:43,556,652-46,084,026	0.99	rs117504376 (3.1×10^{-7})	MAPT (chr17 inversion)	[Estrada et al., 2012] (rs1864325, 0.99)
RBC	chr20:54,899,828-57,013,873	0.96	rs737092 (4.5×10^{-4})	MIR5095	[van der Harst et al., 2012] (rs737092)
MPV	chr14:67,315,438-69,802,709	0.91	rs117823369 (3.9×10^{-6})	DCAF5	NA
FG	chr9:111,051,626-112,662,634	0.96	rs76817627 (3.4×10^{-7})	FAM206A	NA

Table 22: **Sub-threshold associations with high posterior probability.** In each GWAS, we identified regions of the genome with a posterior probability of association greater than 0.9 but with no P-values less than 5×10^{-8} . Shown are the positions of these regions for each trait. See Supplementary Text for details. LD between lead SNPs and replication SNPs was computed from the 1000 Genomes Project haplotypes in Europeans; the exact file versions are listed in Section 3.

References

- Bacanu, S.-A., Devlin, B., and Roeder, K., 2002. Association studies for quantitative traits in structured populations. *Genetic epidemiology*, **22**(1):78–93.
- Estrada, K., Styrkarsdottir, U., Evangelou, E., Hsu, Y.-H., Duncan, E. L., Ntzani, E. E., Oei, L., Albagha, O. M., Amin, N., Kemp, J. P., *et al.*, 2012. Genome-wide meta-analysis identifies 56 bone mineral density loci and reveals 14 loci associated with risk of fracture. *Nature genetics*, **44**(5):491–501.
- Gieger, C., Radhakrishnan, A., Cvejic, A., Tang, W., Porcu, E., Pistis, G., Serbanovic-Canic, J., Elling, U., Goodall, A. H., Labrune, Y., *et al.*, 2011. New gene functions in megakaryopoiesis and platelet formation. *Nature*, **480**(7376):201–208.
- Global Lipids Genetics Consortium, Willer, C. J., Schmidt, E. M., Sengupta, S., Peloso, G. M., Gustafsson, S., Kanoni, S., Ganna, A., Chen, J., Buchkovich, M. L., *et al.*, 2013. Discovery and refinement of loci associated with lipid levels. *Nat Genet*, **45**(11):1274–83.
- Hoffman, M. M., Ernst, J., Wilder, S. P., Kundaje, A., Harris, R. S., Libbrecht, M., Giardine, B., Ellenbogen, P. M., Bilmes, J. A., Birney, E., *et al.*, 2013. Integrative annotation of chromatin elements from ENCODE data. *Nucleic acids research*, **41**(2):827–841.
- Jostins, L., Ripke, S., Weersma, R. K., Duerr, R. H., McGovern, D. P., Hui, K. Y., Lee, J. C., Schumm, L. P., Sharma, Y., Anderson, C. A., *et al.*, 2012. Host-microbe interactions have shaped the genetic architecture of inflammatory bowel disease. *Nature*, **491**(7422):119–124.
- Lango-Allen, H., Estrada, K., Lettre, G., Berndt, S. I., Weedon, M. N., Rivadeneira, F., Willer, C. J., Jackson, A. U., Vedantam, S., Raychaudhuri, S., *et al.*, 2010. Hundreds of variants clustered in genomic loci and biological pathways affect human height. *Nature*, **467**(7317):832–838.
- Manning, A. K., Hivert, M.-F., Scott, R. A., Grimsby, J. L., Bouatia-Naji, N., Chen, H., Rybin, D., Liu, C.-T., Bielak, L. F., Prokopenko, I., *et al.*, 2012. A genome-wide approach accounting for body mass index identifies genetic variants influencing fasting glycemic traits and insulin resistance. *Nature genetics*, **44**(6):659–669.
- Maurano, M. T., Humbert, R., Rynes, E., Thurman, R. E., Haugen, E., Wang, H., Reynolds, A. P., Sandstrom, R., Qu, H., Brody, J., *et al.*, 2012. Systematic localization of common disease-associated variation in regulatory DNA. *Science*, **337**(6099):1190–5.
- Pasaniuc, B., Zaitlen, N., Shi, H., Bhatia, G., Gusev, A., Pickrell, J., Hirschhorn, J., Strachan, D. P., Patterson, N., and Price, A. L., *et al.*, 2013. Fast and accurate imputation of summary statistics enhances evidence of functional enrichment. *arXiv preprint arXiv:1309.3258*, .
- R Core Team, 2013. *R: A Language and Environment for Statistical Computing*. R Foundation for Statistical Computing, Vienna, Austria.

- Speliotes, E. K., Willer, C. J., Berndt, S. I., Monda, K. L., Thorleifsson, G., Jackson, A. U., Allen, H. L., Lindgren, C. M., Luan, J., Mägi, R., *et al.*, 2010. Association analyses of 249,796 individuals reveal 18 new loci associated with body mass index. *Nature genetics*, **42**(11):937–948.
- Teslovich, T. M., Musunuru, K., Smith, A. V., Edmondson, A. C., Stylianou, I. M., Koseki, M., Pirruccello, J. P., Ripatti, S., Chasman, D. I., Willer, C. J., *et al.*, 2010. Biological, clinical and population relevance of 95 loci for blood lipids. *Nature*, **466**(7307):707–713.
- Thurman, R. E., Rynes, E., Humbert, R., Vierstra, J., Maurano, M. T., Haugen, E., Sheffield, N. C., Stergachis, A. B., Wang, H., Vernot, B., *et al.*, 2012. The accessible chromatin landscape of the human genome. *Nature*, **489**(7414):75–82.
- van der Harst, P., Zhang, W., Leach, I. M., Rendon, A., Verweij, N., Sehmi, J., Paul, D. S., Elling, U., Allayee, H., Li, X., *et al.*, 2012. Seventy-five genetic loci influencing the human red blood cell. *Nature*, **492**(7429):369–375.
- Voight, B. F., Kang, H. M., Ding, J., Palmer, C. D., Sidore, C., Chines, P. S., Burt, N. P., Fuchsberger, C., Li, Y., Erdmann, J., *et al.*, 2012. The metabochip, a custom genotyping array for genetic studies of metabolic, cardiovascular, and anthropometric traits. *PLoS Genet*, **8**(8):e1002793.